Main Manuscript for:

Histone deacetylation and cytosine methylation compartmentalize heterochromatic regions in the genome organization of *Neurospora crassa*

Ashley W. Scadden[1], Alayne S. Graybill[1], Clayton Hull-Crew[1], Tiffany J. Lundberg[1], Nickolas M. Lande[1], and Andrew D. Klocko[1]*

[1]University of Colorado Colorado Springs, Department of Chemistry & Biochemistry, Colorado Springs, CO 80918, USA

***Corresponding Author:** Andrew D. Klocko, email: aklocko@uccs.edu

Author Contributions: A.W.S and A.D.K. designed research; A.W.S., A.S.G., C.H-C., T.J.L., N.M.L., and A.D.K. performed research; A.W.S., A.S.G., C.H-C., T.J.L., N.M.L., and A.D.K. analyzed data; and A.W.S., A.S.G., C.H-C., T.J.L., N.M.L., and A.D.K. wrote the paper.

Competing Interest Statement: The authors declare no conflict of interest.

Classification: Biological Sciences, Genetics

Keywords: histone deacetylation, HDAC, heterochromatin, Hi-C, cytosine methylation

Abstract

Chromosomes must correctly fold in eukaryotic nuclei for proper genome function. Eukaryotic organisms hierarchically organize their genomes: in the fungus *Neurospora crassa*, chromatin fiber loops compact into Topologically Associated Domain (TAD)-like structures that are anchored by the aggregation of silent heterochromatic regions. However, insufficient information exists on how histone post-translational modifications, including acetylation, impact genome organization. In Neurospora, the HCHC complex (comprised of the proteins HDA-1, CDP-2, HP1, and CHAP) deacetylates heterochromatic regions, including centromeres: loss of individual HCHC members increases centromeric acetylation and alters cytosine methylation. Here, we evaluate the role of the HCHC complex on genome organization using chromosome conformation capture with high-throughput sequencing (Hi-C) in strains deleted of the *cdp-2* or *chap* genes. CDP-2 loss increases interactions between intra- and inter-chromosomal heterochromatic regions, while loss of CHAP decreases heterochromatic region compaction. Individual HCHC mutants exhibit different patterns of histone post-translational modifications genome-wide: without CDP-2, heterochromatic H4K16 acetylation is increased, yet some heterochromatic regions lose H3K9 trimethylation, which increases interactions between heterochromatic regions; CHAP loss produces minimal acetylation changes but increases heterochromatic H3K9me3 enrichment. Interestingly, loss of both CDP-2 and the DIM-2 DNA methyltransferase causes extensive genome disorder, as heterochromatic-euchromatic contacts increase despite additional levels of H3K9me3. Our results highlight how the increased cytosine methylation in HCHC mutants ensures heterochromatic compartmentalization when silenced regions become hyperacetylated with loss of HDAC activity.

42 **Significance Statement**

43 The mechanisms driving chromosome organization in eukaryotic nuclei, including in the filamentous fungus
44 *Neurospora crassa*, are currently unknown, but histone post-translational modifications may be involved.
45 Histone proteins can be acetylated to form active euchromatin while histone deacetylases (HDACs) remove
46 acetyl marks to form silent heterochromatin; heterochromatic regions cluster and strongly interact in
47 Neurospora genome organization. Here, we show that mutants lacking components of a heterochromatin-
48 specific HDAC (HCHC) causes histone acetylation gains in heterochromatin genome-wide and contact
49 increases between distant heterochromatic loci. HCHC loss also impacts cytosine methylation, and in strains
50 lacking both the HCHC and cytosine methylation, heterochromatic regions interact more with euchromatin.
51 Our results suggest cytosine methylation normally functions to segregate silent and active loci when
52 heterochromatic acetylation increases.

53 **Main Text**

54 **Introduction**

55 Chromosomal DNA must be correctly folded in a eukaryotic nucleus for proper function, including for
56 transcriptional regulation (1–5). This genome organization includes the subnuclear compartmentalization
57 of chromatin (2, 5) where the more open euchromatin is centrally localized and is accessible to transcription
58 machinery, while the densely compacted heterochromatin aggregates at the nuclear periphery possibly
59 preventing RNA polymerase binding (6–9). In euchromatin, long-range loops also form between promoters
60 and distant regulatory sequences, including enhancers or silencers (3, 10). Genome organization is
61 frequently disrupted in human cancers, where improper gene expression occurs following the hijacking of
62 regulatory sequences by promoters (11–13). Given the direct connection between genome organization and
63 function, there is a critical need to understand the factors folding the genome in wild type (WT) nuclei.

64 The organization of an entire genome can be assessed by chromosome conformation capture with high
65 throughput sequencing (Hi-C), in which chromatin is crosslinked, restriction enzyme digested, and ligated,
66 which physically connects interacting DNA strands in a single DNA molecule; the more accurate *in situ* Hi-C
67 ligates interacting regions in the nucleus, thereby generating precise high resolution contact matrices of
68 genome organization with unprecedented clarity (14–16). Hi-C has shown that the genomes of "higher"
69 eukaryotic species are hierarchically organized. At the most basic level, histone octamers wrap ~146
70 basepairs (bp) of DNA to form the nucleosomes comprising chromatin fiber globules ("loops") (17, 18). Loops
71 compact into Topologically Associated Domains (TADs), where chromatin internal to the TAD is more apt to
72 interact (15, 19–21). TADs of similar transcriptional states are compartmentalized, while individual
73 metazoan chromosomes isolate into territories (6, 14, 15, 22–25).

74 Filamentous fungi, like *Neurospora crassa*, are excellent model organisms for understanding eukaryotic
75 genome organization (16, 26–28). The Neurospora genome, typical among fungi, is small, and predominantly
76 haploid (e.g., the Neurospora genome is 4.1 x 10^7 bp) (29), allowing cost-efficient genomic sequencing
77 experiments. The Neurospora genome also contains both euchromatic and heterochromatic loci, with the
78 latter subdivided into permanently-silent constitutive heterochromatin covering repetitive DNA that is
79 adenine-thymine (AT)-rich and gene-poor, and temporarily-silent facultative heterochromatin repressing

80 gene-rich regions (29–32); each type is demarcated by specific histone post-translational modifications
81 (PTMs). As in humans, Neurospora constitutive heterochromatin is enriched with trimethylation of lysine 9
82 on histone H3 (H3K9me3, catalyzed by the **D**IM-5/-7/-9, **C**UL4, **D**DB1$^{dim\text{-}8}$ **C**omplex [DCDC]) and cytosine
83 methylation (5^{m}C), while the di- or trimethylation of lysine 27 on histone H3 (H3K27me2/3) or the ASH1-
84 dependent di-methylation of lysine 36 on histone H3 (H3K36me2) demarcates facultative heterochromatin
85 (30–38). Histone lysines in euchromatin are extensively acetylated by histone acetyltransferases (HATs),
86 including on histone H3 lysine 9 (H3K9ac) or histone H4 lysine 16 (H4K16ac) (39–41). However, unlike
87 metazoans, the machinery catalyzing histone PTMs or 5^{m}C in Neurospora is simplistic, non-redundant, and
88 not required for viability, promoting the use of Neurospora in experiments for understanding chromatin
89 function (32, 38, 42). Importantly, the genomes of filamentous fungi, including that of *Neurospora crassa*, are
90 compacted in a comparable manner to metazoan genomes, with a similar ratio of genome size to nuclear
91 volume as humans (16). Neurospora chromosomes form TAD-like structures, known as "Regional Globule
92 Clusters", comprised of chromatin loops (16, 26, 27). Flanking heterochromatic regions strongly interact to
93 delineate Neurospora TAD-like structures, which promotes multiple euchromatic globules to associate in an
94 uninsulated manner (16, 27). However, as opposed to the chromosome territories seen in metazoans (1, 22,
95 24, 25), fungal chromosomes form a Rabl conformation, in which centromeres bundle independently from
96 telomere clusters at the nuclear periphery (16, 26–28, 43), as directly observed in Neurospora (26–28); this
97 Rabl structure forms weak chromosome territories with extensive inter-chromosomal contacts.

98 Genome organization may depend on individual histone PTMs compartmentalizing chromatin. It is well
99 established that specific histone PTMs define the transcriptional status and accessibility of chromatin (18,
100 44–46), yet given the segregation of euchromatic and heterochromatic regions in the nucleus, the possibility
101 exists that the histone PTMs marking this chromatin could facilitate genome compartmentalization. Recent
102 reports detail how heterochromatic histone PTMs, as well as the proteins that bind these marks, shape
103 genome organization. Notably, H3K9me3 and its cognate binding partner Heterochromatin Protein-1 (HP1),
104 compact heterochromatic regions during fungal asexual growth and facilitate pericentromere clustering
105 during Drosophila zygote genome activation (27, 43, 47). Also, sub-telomeric H3K27me2/3 facilitates the
106 telomere cluster – nuclear periphery association in Neurospora (26). However, little information exists about

107 the roles of other histone PTMs, including histone acetylation.

108 Classically, acetylated histone tails denote open chromatin, as enrichment of acetylation is observed in
109 in the euchromatic regions of fungi, fruit flies, mice, and humans (33, 48–57). In contrast, heterochromatin
110 is typically devoid of histone acetylation; histone deacetylase (HDAC) complexes remove acetyl marks (33,
111 39, 40, 58). Changes in acetylation levels within chromatin may impact genome organization, with promoter
112 – enhancer interactions being subject to this regulation. Recent reports highlight the acetylation changes of
113 lysine 27 on histone H3 (H3K27ac) across enhancers during the differentiation of human epidermal cells
114 (59) and mouse adipocyte cells (60). Histone acetylation changes are also well-documented during the cell
115 cycle: mitotic chromosomes are globally hypoacetylated to form dense chromosome structures prior to
116 separation into daughter cells (61–65). Specifically during mitosis, promoters and enhancers lose H3K27ac,
117 but rapidly regain this mark in G1 for reactivating gene transcription and reforming TADs (66, 67). Further,
118 the BRD4-NUT novel oncogenic protein recruits the HAT P300 to create hyperacetylated Mega-domains that
119 aggregate into a transcriptionally activated sub-compartment (68); phase-separation might promote nuclear
120 sub-compartment formation (69). While hyperacetylated chromatin may impact genome organization, little
121 is known about how HDAC complex activity affects fungal chromosome conformation.

122 *Neurospora crassa* encodes four class II HDACs (HDA-1 to HDA-4; class characterization based on
123 primary structure conservation), with HDA-1 impacting heterochromatin (41, 58). HDA-1 is a component of
124 the four-member HCHC complex, comprised of the proteins HDA-1, CDP-2 (***C***hromo***d***omain ***P***rotein-***2***), HP1,
125 and CHAP (***C***DP-2 and ***H***DA-1 ***A***ssociated ***P***rotein) (39, 40). HDA-1 is the deacetylase catalytic subunit, HP1
126 binds to H3K9me3 for heterochromatin recruitment, CDP-2 facilitates protein interactions between HP1 and
127 HDA-1 within the HCHC, and CHAP binds to the AT-rich DNA of constitutive heterochromatin, mediated by
128 the two AT hook domains in its primary structure (39, 40). Both CDP-2 and CHAP are necessary to recruit
129 HDA-1 to heterochromatic genomic loci (39). Strains deleted of *cdp-2*, *chap*, or *hda-1* have increased histone
130 acetylation and decreased H3K9me3 at select heterochromatic loci, as assessed by Chromatin
131 Immunoprecipitation (ChIP) quantitative PCR, although it is unknown if these changes occur genome-wide
132 (40). Also, smaller heterochromatic regions in HCHC mutant strains lose $5^{m}C$ but larger regions, including
133 centromeres, gain $5^{m}C$ by increasing recruitment of DIM-2, the only DNA methyltransferase encoded in

134 Neurospora (39). Thus, HCHC mutants have distinct changes in histone PTMs and 5^{m}C that might impact
135 genome organization.

136 Here, we report how the HCHC complex impacts genome organization using Δ*cdp-2* and Δ*chap* deletion
137 strains. CDP-2 loss increases intra- and inter-chromosomal heterochromatic region contacts, while loss of
138 CHAP reduces heterochromatic region compaction. Heterochromatic regions gain H4K16ac but not H3K9ac
139 enrichment; a Δ*chap* strain has little H4K16ac change. Surprisingly, some heterochromatic regions lose
140 H3K9me3 in a Δ*cdp-2* strain, which causes contact promiscuity of affected heterochromatic regions.
141 Moreover, a Δ*cdp-2*;Δ*dim-2* double mutant devoid of 5^{m}C in an HCHC-deficient background gains H3K9me3
142 at most AT-rich regions and has a highly disordered genome organization, with increased contact
143 probabilities between heterochromatic loci and euchromatin. Our results suggest that histone deacetylation
144 is required for Neurospora genome organization, while in the presence of hyperacetylated histones, 5^{m}C
145 maintains the segregation of heterochromatin from euchromatin.

146

147 **Results**

148 *Genome organization changes in strains deleted of either HCHC component CDP-2 or CHAP*

149 The genome of the wild type (WT) *Neurospora crassa* strain N150 (74-OR23-IVA [Fungal Genetic Stock
150 Center #2489]) is organized by heterochromatin aggregates, which form euchromatic TAD-like structures
151 (Figure 1A) (16, 26–28). Heterochromatic regions in the Neurospora genome depend on the action of the
152 HDAC complex HCHC for 5^{m}C and silencing (40). To understand if the HCHC also mediates Neurospora
153 genome organization, we examined strains independently deleted of the genes encoding CDP-2 (Δ*cdp-2*) or
154 CHAP (Δ*chap*) by *in situ* Hi-C. Since CDP-2 and CHAP recruit HDA-1 to AT-rich genomic loci for histone
155 deacetylation, the activity of CDP-2 and CHAP may be epistatic to HDA-1 action, yet given the unique domains
156 predicted from their primary structures, these proteins could have distinct functions in the HCHC complex
157 (39, 40). We hypothesized that by examining mutants of CDP-2 and CHAP, we would assess how
158 compromised HCHC function alters chromosome conformation and observe more nuanced differences in
159 genome organization to clarify the individual roles of these HCHC members, rather than only examining the

160 effect of deleting the HDA-1 catalytic subunit. Therefore, we independently performed chromatin-specific *in*
161 *situ* Hi-C with *Dpn*II (recognition sequence ^GATC) to assess euchromatic contacts, or *Mse*I (T^TAA) to
162 examine heterochromatic interactions, on Δ*cdp-2* and Δ*chap* strains. Our replicate *in situ* Hi-C libraries,
163 generated from a population of cells, are highly reproducible (Figures S1, S2), allowing similar restriction
164 enzyme datasets to be merged. This produced high quality *Dpn*II Δ*cdp-2* (~35.4 million [M] valid read pairs)
165 and Δ*chap* (~8.7M valid read pairs), as well as *Mse*I Δ*cdp-2* (~13.9M valid read pairs) and Δ*chap* (~4.8M valid
166 read pairs) datasets; total and valid read counts are provided in Supplemental Table S1. The merged *Dpn*II
167 datasets presented are Knight-Ruiz (KR) corrected to limit experimental bias (22, 70, 71), while *Mse*I datasets
168 show raw read counts, since KR correction improperly removes heterochromatic region contacts upon bin
169 averaging, possibly due to the discrepancy of *Mse*I site numbers between AT-rich heterochromatin and GC-
170 rich euchromatin (16).

171 At first glance, when examining a single chromosome (Linkage Group [LG] II), the *Dpn*II and *Mse*I Δ*cdp-2*
172 datasets (Figures 1B) look comparable to WT *Dpn*II or *Mse*I Hi-C datasets (Figure 1A), the latter generated
173 from fastq files containing nearly identical numbers of valid reads. However, upon closer examination, the
174 Δ*cdp-2* dataset has increased interactions between distant heterochromatic regions, including the LG II
175 centromere, which forms prominent interactions with heterochromatic regions up to three Megabases (Mb)
176 distant, as evident in the heterochromatin-specific *Mse*I heatmap (Figure 1B, black arrowheads), while
177 heterochromatic regions form fewer contacts with nearby euchromatin (Figure 1B, open arrowheads). These
178 effects are seen across all Neurospora chromosomes (Figures S3). To highlight changes in a Δ*cdp-2* strain,
179 we directly compared the *Dpn*II or *Mse*I Δ*cdp-2* Hi-C contact maps to those from a WT strain. In both datasets,
180 the most prominent change in LG II interactions in Δ*cdp-2* are the strong increases between centromeres and
181 distant heterochromatic regions, evident as strong red bins in comparison heatmaps (Figure 1C); a similar
182 pattern is observed for all seven Neurospora LGs (Figures S4). Further examination of the high-resolution
183 contact changes at centromeres show how centromeric chromatin is more accessible in a Δ*cdp-2* strain, as
184 the LG II centromere has a strong red diagonal indicative of increased contacts between centromeric
185 nucleosomes, in addition to having more intense interactions with distant H3K9me3-marked constitutive
186 heterochromatic regions (Figure 1D). In fact, each heterochromatic region across LG II has increased local

187 interactions along the diagonal of Δ*cdp-2 Mse*I datasets relative to WT, arguing this AT-rich, heterochromatic
188 DNA associates less with its own histone proteins for greater contact promiscuity with the DNA of nearby
189 heterochromatic nucleosomes; this could additionally deplete heterochromatic-euchromatic contacts when
190 equal numbers of valid Hi-C read pairs are compared (Figures 1B, open arrowheads, 1C). Quantification of
191 strongly changed contacts between WT and Δ*cdp-2 Mse*I datasets showed that, indeed, the greatest number
192 of strongly increased contacts occurred between H3K9me3-enriched bins; few contacts are strongly
193 increased between H3K9me3 enriched bins and bins enriched with euchromatic marks (Figure 1E).
194 Furthermore, as assessed in *Dpn*II datasets, interactions of distant euchromatic regions are decreased, such
195 that interactions between the left and right chromosome arms, as well as the interactions between distant
196 TAD-like structures are reduced (Figure 1C). The strong decrease in off diagonal interactions when
197 comparing the WT and Δ*cdp-2 Mse*I datasets (Figure 1C, above diagonal) could indicate chromatin in TAD-
198 like structures interact less, similar to the changes in *Dpn*II Δ*cdp-2* datasets, but equally possible is that this
199 decrease in euchromatic interactions reflects contact paucity caused by the reduced number of *Mse*I sites in
200 euchromatin (16) coupled with the above increase in heterochromatin-specific contacts (Figure 1C). All told,
201 CDP-2 loss increases constitutive heterochromatin interactions and decreases euchromatin contacts.

202 Next, we examined the genome organization of a Δ*chap* strain by *Dpn*II and *Mse*I Hi-C. The Δ*chap* data
203 has reduced valid read numbers, with the Δ*chap Dpn*II dataset having ~four-fold less reads and the Δ*chap*
204 *Mse*I dataset having ~three-fold less valid reads compared to Δ*cdp-2* (Supplemental Table S1). However,
205 despite these valid read number differences, we believe enough information is present to assess the impact
206 of CHAP loss, especially considering WT datasets are normalized with similar valid read numbers for all
207 Δ*chap* dataset comparisons. Examination of single chromosomes show how the Δ*chap Dpn*II and *Mse*I Hi-C
208 datasets appear devoid of most strong long-range contacts (Figure 1F); similar results were shown for all
209 seven Linkage Groups (Figure S5). In each chromosome, more distant contacts are rarer upon CHAP loss; an
210 enhanced image of the right arm of LG II highlights that regional interactions still form in both *Dpn*II and *Mse*I
211 datasets (Figure S6). When equal numbers of valid reads between WT and Δ*chap* datasets are compared,
212 heterochromatic regions exhibit reduced internal compaction, and fewer contacts between heterochromatic
213 regions across LG II are observed (Figures 1G, S6B; arrowheads); similar differences occur on each

214 chromosome upon CHAP loss (Figure S7). Also apparent are the decreased interactions between the TAD-
215 like Regional Globule Clusters (16) in the Δ*chap Dpn*II data, which may stem from the slight increase in on-
216 diagonal, local interactions (Figures 1G, S6-S7). Quantification of strongly increased contacts between bins
217 enriched for either activating or repressive histone PTMs, including the SET-2-specific H3K36me2 or
218 H3K27ac (33), shows minimal gains in bin interactions between heterochromatic and euchromatic bins, yet
219 euchromatic regions are more likely to contact in Δ*chap* (Figure 1E), perhaps indirectly resulting from
220 decreased heterochromatic compaction.

221 Similar interaction trends are observed across the entire Neurospora genome, arguing that CDP-2 and
222 CHAP mediate the inter-chromosomal clustering of Neurospora heterochromatic regions. As shown in raw
223 *Mse*I and KR corrected *Dpn*II Hi-C data from a Δ*cdp-2* strain, or when these Δ*cdp-2* data are compared to WT
224 Hi-C, the centromeres in a Δ*cdp-2* strain gain interactions with the interspersed heterochromatic regions
225 across all seven LGs, thereby reducing contact strength of the centromere-proximal euchromatin on each
226 chromosome and the inter-chromosomal centromeric interactions (Figures S8-S9), although it is possible
227 this reduction manifests when equal valid read pair numbers are compared between datasets in which one
228 (Δ*cdp-2*) has more heterochromatin contacts. The Δ*cdp-2 Dpn*II Hi-C data present with stronger inter-
229 chromosomal arm contacts (Figure S9), which may occur when heterochromatic regions between
230 chromosomes more strongly interact; similar changes are observed in KR-corrected *Mse*I data and raw *Dpn*II
231 data when WT and Δ*cdp-2* contact matrices are compared (Figure S10A). Examination of the interactions
232 between two chromosomes, LG II and LG III, in Δ*cdp-2 Mse*I Hi-C contact heatmaps show the expansion of
233 centromeric and interspersed heterochromatic region contacts and the concomitant reduction of contacts
234 between silent and active chromatin (Figure S8A). Plotting the inter-chromosomal interaction changes
235 between WT and Δ*cdp-2 Mse*I datasets highlight how inter-chromosomal heterochromatic regions are more
236 apt to interact, including the LG II and LG III centromeres strongly contacting distant heterochromatic
237 regions (Figure 2A). Decreased contacts include the inter-centromeric and pericentromeric euchromatin
238 (Figure 2A). CHAP loss reduces heterochromatic interactions across the Neurospora genome: as shown in
239 Δ*chap Mse*I contact matrices (Figure S11), or when Δ*chap Mse*I data is compared to WT *Mse*I data (Figure
240 S9B), few inter-chromosomal heterochromatic contacts are observed, with the reduction in centromeric

241 contacts being the most prominent; these contact strength differences are independent of matrix correction
242 (Figure S10B). A plot of the interactions between LG II and LG III in Δ*chap* highlights the paucity of inter-
243 chromosomal constitutive heterochromatic contacts (Figure S11A), which is further evident when *Mse*I Hi-C
244 data between a WT and Δ*chap* strain are compared (Figure 2B). The decrease in heterochromatic bundling
245 compromises the inter-chromosomal arm interactions characteristic of the Rabl conformation (28), as the
246 comparison of *Dpn*II Hi-C between WT and Δ*chap* strains shows reduced euchromatin interactions across
247 the left and right chromosomal arms (Figure S10B). Quantification of the strongest gains in inter-
248 chromosomal interactions in HCHC deletion mutants, relative to WT, shows inter-bin interactions are gained
249 in 81.5% of H3K9me3 enriched bins, but few heterochromatic-euchromatic bins gain contacts, in Δ*cdp-2 Mse*I
250 datasets (Figure 2C, left). The Δ*cdp-2 Dpn*II Hi-C data only show strong gains between euchromatic bins
251 enriched with H3K27ac and SET-2 specific H3K36me2 (Figure 2C, right). In contrast, Δ*chap Mse*I and *Dpn*II
252 Hi-C datasets have minimal contact increases relative to WT, independent of histone PTMs, consistent with
253 the loss of CHAP reducing heterochromatic interactions (Figure 2C).
254 Our data suggest that CDP-2 and CHAP differentially impact genome organization. To highlight these
255 differences, we compared equal valid read numbers from Δ*cdp-2* and Δ*chap* datasets; Figure S12 shows how
256 genome topology is changed in a Δ*chap* strain relative to Δ*cdp-2*. In these heatmaps, the decrease in
257 heterochromatin compaction and inter-heterochromatic region contacts, with the concomitant increase in
258 euchromatic interactions, that occur upon loss of CHAP is evident (Figure S12C, arrowheads). These data
259 argue that CHAP forms intra-chromosomal interactions within and between heterochromatic regions, while
260 CDP-2 may be indirectly acting to restrict heterochromatin aggregation, given its role in controlling histone
261 acetylation (below). All told, our Δ*cdp-2* and Δ*chap* Hi-C data reveal the differential effects on genome
262 organization by individual members of a histone deacetylase complex.
263
264 *Histone acetylation changes in single deletion strains of the HCHC components CDP-2 and CHAP*
265 To understand how altered HCHC function affects fungal genome organization, we decided to correlate
266 changes in genome organization to histone acetylation enrichment in Δ*cdp-2* and Δ*chap* strains. However, no
267 genome-wide Chromatin Immunoprecipitation (ChIP) sequencing (ChIP-seq) datasets of HCHC mutants are

268 publicly available to make this assessment; recent work showing histone acetylation changes in Δ*cdp-2* and
269 Δ*chap* strains only used ChIP qPCR to show that loss of CDP-2 and CHAP locally increase histone acetylation
270 levels at a few heterochromatic loci (40), preventing genome-wide conclusions or correlation to genome
271 organization. Therefore, we performed two ChIP-seq replicates of histone acetylation on two lysine residues,
272 K9 on histone H3 (H3K9ac) and K16 on histone H4 (H4K16ac), in Δ*cdp-2* and WT strains; we also performed
273 H4K16ac ChIP-seq on a Δ*chap* strain. Both H3K9ac and H4K16ac were proposed to be targets of the HCHC
274 complex, as assessed by ChIP qPCR (40). Our H3K9ac and H4K16ac ChIP-seq replicates are qualitatively
275 reproducible in each strain (Figure S13, S14), so we merged H3K9ac or H4K16ac replicates for Integrative
276 Genome Viewer (IGV) display (72); all ChIP-seq data here are normalized by Reads Per Kilobase per Million
277 reads (RPKM) to ensure proper comparison between each experiment, although the use of spike-in DNA (73–
278 75) might have detected additional enrichment changes. Consistent with the published qPCR ChIP, CDP-2
279 loss caused an increase in H4K16ac enrichment only in AT-rich heterochromatic regions but had little effect
280 on H3K9ac enrichment (Figure 3A, top). Closer examination of the LG II right arm highlights this acetylation
281 change, as each H3K9me3-marked heterochromatic region gains H4K16ac relative to WT, but H3K9ac is not
282 enriched (Figure 3A, bottom, arrowheads), possibly reflecting the trimethylation of this residue in these
283 gene-poor regions (Figure 3A, dark green track). The enrichment of H4K16ac and H3K9ac in a Δ*cdp-2* strain
284 was unchanged in gene-rich euchromatin (Figure 3A), highlighting how the HCHC complex may be specific
285 for deacetylating only AT-rich heterochromatic regions in the Neurospora genome. In contrast, the loss of
286 CHAP had little effect on acetylation: the Δ*chap* strain showed minimal, if any, changes to the enrichment of
287 H4K16ac across genes and within constitutive heterochromatic regions (Figure S15A).

288 These acetylation changes are highlighted by average enrichment plots and heatmaps of the normalized
289 H4K16ac and H3K9ac datasets across either H3K9me3-enriched regions or genes. Over heterochromatic
290 regions, the gain of H4K16ac is readily apparent, as essentially all AT-rich regions have a substantial increase
291 in H4K16ac enrichment in a Δ*cdp-2* strain relative to the minimal heterochromatic H4K16ac in a WT strain
292 (Figure 3B). In contrast, the enrichment of H3K9ac in the heterochromatic regions of a Δ*cdp-2* strain may be
293 slightly lower than a WT strain (Figure S16A). The Δ*chap* strain has only a subtle increase in H4K16ac across
294 heterochromatin (Figure S15B), highlighting the possible differences in individual HCHC components for

295 deacetylation. When examining H4K16ac over genes, a Δ*cdp-2* strain has a small reduction in H4K16ac
296 compared to the WT strain (Figure S17A), suggesting that increases in heterochromatic nucleosome
297 acetylation limits the level of genic acetylation in euchromatin by HAT(s). Similarly, H3K9ac deposition
298 across genes subtly shifts from the 5' end of genes in a Δ*cdp-2* strain (Figure S16B). To further characterize
299 the H4K16ac and H3K9ac deposition changes, we plotted the normalized, averaged signal of each region
300 using boxplots. The heterochromatic regions in Δ*cdp-2* have robust increases in H4K16ac signal relative to
301 WT (Figure S17B), while H3K9ac enrichment is overall decreased (Figure S16C), although some regions in
302 each dataset go against these trends. Considering genic acetylation, a Δ*cdp-2* strain has a small but
303 statistically significant H4K16ac decrease (Figure S17C) and H3K9ac increase (Figure S16D). Together,
304 HCHC loss differentially effects enrichment of histone acetylation across the Neurospora genome.
305
306 *Changes in H3K9me3-deposition and heterochromatin bundling in* Δcdp-2 *and* Δchap *strains*
307 Given the gain in constitutive heterochromatic acetylation in HCHC mutants, we examined H3K9me3
308 enrichment by ChIP-seq to assess possible differences in permanently silent genomic loci in Δ*cdp-2* and
309 Δ*chap* strains. The H3K9me3 ChIP-seq replicates of each strain are reproducible (Figure S18), allowing us to
310 merge the replicates from each strain. H3K9me3 enrichment in a Δ*cdp-2* strain resembles that of a WT strain:
311 most regions have similar levels of H3K9me3 deposition (Figure 3A). However, several moderately sized
312 heterochromatic regions in WT have a near-complete or total loss of H3K9me3 in a Δ*cdp-2* strain (Figures
313 3A and S19A, asterisks), while nearby heterochromatic regions still retain normal H3K9me3 levels. Zooming
314 into one affected region, we observe background levels of H3K9me3 across the entire locus, indicating read
315 mapping is unaffected, which argues against underlying DNA changes in regions losing H3K9me3 (Figure
316 S19A, red box). In contrast, the loss of CHAP causes a subtle gain in H3K9me3 in most heterochromatic
317 regions relative to WT, even with RPKM normalization, (Figure S15A). Average enrichment plots and
318 heatmaps highlight the H3K9me3 changes in Δ*cdp-2* and Δ*chap* strains, with most heterochromatic regions,
319 but not genes, gaining H3K9me3 enrichment with loss of CHAP (Figure S15D-E). Conversely, while many
320 heterochromatic regions are unchanged with CDP-2 loss, some AT-rich loci have a reduction, or a complete
321 loss of, H3K9me3 (Figure 3C). Boxplots of average signal across heterochromatic regions also highlight this

322 change, with lower normalized H3K9me3 signals across all AT-rich regions in a Δ*cdp-2* strain (Figure S19B).
323 We hypothesized that the H3K9me3 loss and H4K16ac gain might affect the genome organization of these
324 formerly heterochromatic regions. To this end, we plotted the Hi-C contact probability changes between WT
325 and Δ*cdp-2* datasets across two regions on LG I and LG III, each of which encompass AT-rich regions losing
326 H3K9me3 in a Δ*cdp-2* strain (Figures 3D, S19C). In both instances, regions losing H3K9me3 strongly gain
327 contacts with other AT rich regions retaining this silencing mark. For example, on LG I, the loss of H3K9me3
328 from (and concomitant gain of H4K16ac in) multiple AT-rich loci caused gains in inter-region contacts; pairs
329 of other nearby regions that retain H3K9me3 are unaffected (Figure 3D, closed arrowheads). Also, on LG III,
330 the contacts between two nearby AT-rich genomic regions are increased when one region loses H3K9me3,
331 while two other similarly sized heterochromatic regions have few long-range interaction changes (Figure
332 S19C, compare closed and open arrowheads). All told, the loss of CDP-2 impacts histone PTM enrichment,
333 which causes the typically heterochromatic AT-rich genomic loci to form a more open chromatin structure
334 for increased contact probability with other heterochromatic regions in the silent chromatin bundle.
335
336 *Changes in histone PTMs and genome organization in a* Δcdp-2;Δdim-2 *double mutant*
337 To this point, we have shown that the heterochromatic regions of strains individually deleted of HCHC
338 complex members gain acetylation, which alters H3K9me3 deposition and silent chromatin bundling.
339 However, CDP-2 or CHAP loss also alters the deposition of cytosine methylation: centromeres and other large
340 interspersed heterochromatic regions gain $5^{m}C$, while small AT-rich regions lose $5^{m}C$ (39, 40).
341 Hypothetically, extra $5^{m}C$ in a heterochromatic region in any HCHC mutant, including a Δ*cdp-2* strain, may
342 confer additional properties to AT-rich loci, meaning $5^{m}C$ gains must be considered when assessing genome
343 organization. In support, a Δ*cdp-2*;Δ*dim-2* strain, in which the gene encoding the only DNA methyltransferase
344 in Neurospora is deleted in a Δ*cdp-2* background, has a compromised growth rate relative to single HCHC
345 mutants (40).
346 To understand if an increase in $5^{m}C$ alters histone PTM deposition following HCHC complex loss, we
347 examined levels of H4K16ac and H3K9me3 in a Δ*cdp-2*;Δ*dim-2* double mutant strain. Our ChIP-seq replicate
348 experiments are qualitatively comparable (Figures S14, S18), allowing us to merge identical histone PTM

349 replicates; as before, all ChIP-seq tracks are RPKM normalized. Compared to Δ*cdp-2*, the H4K16ac
350 distribution in a Δ*cdp-2*;Δ*dim-2* strain is essentially unchanged (Figure 4A-B, blue tracks), where both mutant
351 strains gain heterochromatic H4K16ac with minimal changes to genic acetylation (Figure 4A-B), suggesting
352 that DIM-2 loss marginally alters AT-rich DNA hyperacetylation. Boxplots of the normalized average signal
353 across heterochromatic regions show a Δ*cdp-2*;Δ*dim-2* strain has slightly reduced H4K16ac relative to a
354 Δ*cdp-2* single mutant but still strongly increased relative to WT H4K16ac enrichment (Figure S20A). Further,
355 most AT-rich regions in a Δ*cdp-2*;Δ*dim-2* strain strongly gain H3K9me3 when compared to WT and Δ*cdp-2*
356 strains (Figures 4A, 4C). However, the same ~20% of AT-rich regions completely lack H3K9me3 in both the
357 Δ*cdp-2* and double mutant strains (Figures 4A, asterisks, 4C), suggesting the underlying DNA sequence of
358 individual AT-rich regions occlude H3K9me3 deposition. Boxplots of the averaged H3K9me3 enrichment of
359 AT-rich regions highlights the substantial increase in H3K9me3 signal in a Δ*cdp-2*;Δ*dim-2* strain (Figure
360 S20B). Thus, histone acetylation gains coupled with $5^{m}C$ loss at AT-rich loci signals for increased H3K9me3
361 by the DCDC (38).

362 To assess if enhanced heterochromatic acetylation coupled with $5^{m}C$ loss impacts genome organization,
363 we performed euchromatin-specific (*Dpn*II) *in situ* Hi-C to generally assess genome organization of the Δ*cdp-*
364 *2*;Δ*dim-2* strain. We generated two highly correlated *in situ Dpn*II Hi-C replicates of a Δ*cdp-2*;Δ*dim-2* strain
365 (Figure S21), which we merged into a single *Dpn*II Δ*cdp-2*;Δ*dim-2* Hi-C dataset containing 23.1M valid read
366 pairs (Table S1). The contact frequency heatmap for the Δ*cdp-2*;Δ*dim-2* strain shows some segregation of
367 heterochromatic regions from euchromatin, as observed across each individual chromosome (Figure S22)
368 or the entire genome (Figure S23). The whole genome contact probability heatmap also shows centromere
369 bundles independent of telomere clusters typical of the Rabl conformation (Figure S23B), indicating that the
370 overall genome organization of the Δ*cdp-2*;Δ*dim-2* strain is maintained.

371 However, comparison of equal numbers of valid read pairs between the Δ*cdp-2*;Δ*dim-2* and WT *Dpn*II Hi-
372 C datasets showed strong genome organization changes in the double mutant, with heterochromatic regions
373 in Δ*cdp-2*;Δ*dim-2* interacting more with surrounding euchromatin. Both raw and KR corrected heatmaps
374 comparing WT and Δ*cdp-2*;Δ*dim-2* contact probabilities show that AT-rich (formerly heterochromatic) loci,
375 including the centromere, gain interactions with flanking euchromatic DNA across all LGs (Figure S24),

376 including LG II (Figure 5A). Notably, the increased interactions between heterochromatic regions evident
377 upon CDP-2 loss (e.g., Figures 1B-D) is not apparent in a Δ*cdp-2*;Δ*dim-2* strain, suggesting heterochromatin
378 can cluster, as in WT, but the inter-heterochromatic contact gains are abrogated by 5^{m}C loss. In addition,
379 obvious reductions in local and regional euchromatic interactions are observed (Figure 5A), suggesting
380 normal genic contacts are less likely to form, possibly explaining the growth deficiency of a Δ*cdp-2*;Δ*dim-2*
381 strain. Quantification of the strongly changed intra-chromosomal interactions in the Δ*cdp-2*;Δ*dim-2* dataset
382 relative to the WT dataset show more H3K9me3 enriched bins as gaining contacts, often to bins enriched for
383 euchromatic histone PTMs; greater numbers of bins enriched for euchromatic marks also strongly gain
384 contacts in the double mutant (Figure 5B). These contact probability increases between heterochromatic and
385 euchromatic regions also occur across the whole genome, independent of KR correction, which manifest as
386 inter-chromosomal contact gains that deplete the weak chromosome territories typically observed in WT
387 datasets (Figure S25). Quantifying the strongly increased inter-chromosomal contacts shows interaction
388 gains between heterochromatic and euchromatic bins, as well as interactions between two euchromatic bins
389 (Figure 5B). Together, we conclude that the heterochromatin bundle of a Δ*cdp-2*;Δ*dim-2* strain is less
390 compact and more promiscuous following the gains in histone acetylation and the loss of 5^{m}C.

391 We compared the *Dpn*II Hi-C data of the Δ*cdp-2* single mutant and the Δ*cdp-2*;Δ*dim-2* double mutant to
392 highlight the genome organization changes caused by hyperacetylation and 5^{m}C loss. Across LG II, the Δ*cdp-*
393 *2*;Δ*dim-2* strain presents an altered genome topology relative to the Δ*cdp-2* strain, with perhaps stronger
394 gains in contact frequency between heterochromatic and euchromatic regions, increases in regional
395 euchromatic contacts across TAD-like structures, and decreased local (on-diagonal) contacts (Figure 5C).
396 Similar changes in contact frequency when comparing Δ*cdp-2* and double mutant data are seen across the
397 other LGs and over the entire Neurospora genome (Figures S26, S27). Closer examination of the regional
398 contact changes between AT-rich loci and euchromatin highlight how loss of both CDP-2 and DIM-2 impacts
399 chromosome conformation: relative to WT, individual H3K9me3-enriched loci more strongly contact
400 euchromatin, thereby depleting euchromatic clustering; this phenotype is exacerbated in a Δ*cdp-2*;Δ*dim-2*
401 and Δ*cdp-2* contact probability comparison (Figure 5D). We conclude that heterochromatic hyperacetylation
402 and 5^{m}C loss compromises the normal chromosome conformation in Neurospora nuclei.

403

404 **Discussion**

405 In this work, we examined the role of CDP-2 and CHAP, as members of the constitutive heterochromatin-
406 specific histone deacetylase complex HCHC, in modulating histone PTM enrichment and organizing the
407 genome of the filamentous fungal model organism *Neurospora crassa*. We found that increased
408 heterochromatic acetylation in a Δ*cdp-2* strain causes gains in distant intra- and inter-chromosomal
409 heterochromatic contacts, while the loss of CHAP manifests with reduced heterochromatic region
410 aggregation without strong changes in histone acetylation, although neither gene deletion destroyed the Rabl
411 chromosome conformation typical of fungal genomes (28), suggesting genome organization can still form
412 despite HCHC loss. Overall, these data suggest that CDP-2 and CHAP have unique and distinct functions in
413 the HCHC complex that differentially impact genome organization. Our model (Figure 6) is that CDP-2
414 recruits the HDA-1 deacetylase to properly compact individual heterochromatic regions for normal genome
415 organization while CHAP mediates heterochromatic region clustering prior to deacetylation. Specifically, the
416 increased acetylation seen with CDP-2 loss would open chromatin fibers and/or loosen the DNA wrapped
417 about histones in heterochromatic nucleosomes to facilitate distant contacts within the silent "B"
418 compartment at the nuclear periphery (14). In contrast, CHAP would compact heterochromatic regions into
419 dense structures to facilitate inter-heterochromatic region contacts, possibly through its AT-hook motifs that
420 directly bind AT-rich DNA (39). Since both proteins are required to recruit the HDA-1 catalytic subunit to
421 heterochromatin (39), CDP-2 and CHAP must act prior to HDA-1, and the genome organizational changes we
422 observe reflect deficient HDA-1 targeting or the complete loss of HCHC complex formation/function. Notably,
423 the loss of the fourth HCHC complex member, HP1 (in Δ*hpo* strain Hi-C datasets), has a genome organization
424 distinct from that of Δ*cdp-2* or Δ*chap* strains, as the flanking euchromatin emanating from heterochromatic
425 regions have reduced contact probabilities in WT vs. Δ*hpo* datasets, similar to that of a Δ*dim-5* strain lacking
426 H3K9me3 (27). Therefore, HP1 binding to H3K9me3 most likely occurs prior to, or in parallel with, CHAP
427 condensing AT-rich regions; CHAP and HP1 could both act prior to CDP-2 binding HP1 for HDA-1 recruitment
428 (39). This proposed mechanism for Neurospora HCHC activity may be homologous to yeast HDAC complexes.
429 In *Saccharomyces cerevisiae*, Sirtuin-2 (Sir2; a Class III HDAC)-specific deacetylation is required for the

430 binding of the Sir3/Sir4 dimer onto deacetylated histone tails to form silenced superstructures at
431 heterochromatic loci across the budding yeast genome (50, 58, 76, 77). *S. cerevisiae* also employs the HDACs
432 Rpd3 (Class I) and HDA-1 (Class II) for euchromatic deacetylation (58, 78–80); Rpd3 forms two distinct
433 HDAC complexes, the Rpd3L (large) and Rpd3S (small) complexes that differ in genomic targets, with Rpd3L
434 deacetylating promoters while Rpd3S deacetylates gene bodies (80–82). In *Schizosaccharomyces pombe*,
435 SHREC (***S***nf2/***H***dac-containing ***Re***pressor ***C***omplex) is a multisubunit HDAC targeted to heterochromatic loci
436 by the HP1-homolog Swi6 for transcriptional gene silencing, although SHREC can localize to euchromatin
437 independent of Swi6 (83–85); the Clr3 catalytic subunit in SHREC is homologous to HDA-1 in Neurospora.
438 Three other HDA paralogs and a Rpd3 homolog, among others, exist in Neurospora (41). Notably, we used
439 the general HDAC inhibitor Trichostatin A (TSA) to examine possible roles of HDAC(s) in WT genome
440 organization, yet TSA severely compromised WT growth, suggesting HDAC paralogs influence fungal genome
441 function. Examination of other HDAC s in Neurospora by Hi-C or ChIP-seq could elucidate how HDAC
442 paralogs impact chromosome conformation or histone PTM deposition.

443 As previously shown by ChIP qPCR, multiple histone lysines become hyperacetylated upon loss of the
444 HCHC members HDA-1 and CDP-2; the extent of the acetylation changes depends on which heterochromatic
445 region was assessed as well as which HCHC member was deleted (40). However, this published ChIP qPCR
446 data also hints at the HCHC complex having preferential deacetylation activity for certain lysine residues
447 over others. Our ChIP-seq data provides a genome-wide view of the different acetylation patterns in Δ*cdp-2*
448 and Δ*chap* backgrounds, with a Δ*cdp-2* strain becoming hyperacetylated at H4K16 but minimally changed at
449 H3K9 in heterochromatic regions genome wide, while H4K16ac enrichment is minimally altered in a Δ*chap*
450 strain. These data suggest the HCHC complex specifically deacetylates certain heterochromatic histone acetyl
451 marks. It remains possible that HP1, or even CDP-2, both of which can bind to H3K9me3 (40, 86, 87), can
452 compensate for CHAP loss for HDA-1 deacetylation. However, the unchanged levels of H3K9ac in a Δ*cdp-2*
453 strain most likely reflects tri-methylation of that residue by the DCDC in these strains (38), given the mutually
454 exclusive deposition of either acetylation or trimethylation on the lysine residue at position 9 on histone H3
455 (88, 89). Future ChIP-seq experiments on other individual histone lysine residues in Δ*cdp-2,* Δ*chap*, or Δ*hda-*
456 *1* strains should provide global patterns of acetylation changes to dissect HCHC lysine specificity.

457 Interestingly, while Δ*cdp-2* or Δ*chap* strains gain heterochromatin-specific H4K16ac relative to WT, these
458 mutant strains display no change in euchromatic acetylation, suggesting the HCHC complex specifically
459 deacetylates heterochromatic histones. Since both the class II HDAC HDA-1 in Neurospora and the class III
460 HDACs Hst2p and Sir2 in *S. cerevisiae* are both known to deacetylate H4K16 (63, 77), yet they share little
461 primary structure similarity, it is possible that different HDACs are capable of deacetylating the same histone
462 lysines, while the targeting mechanism of individual HDAC complexes determines which genomic loci are
463 deacetylated. Given that HDA-1 is targeted to heterochromatic nucleosomes by CHAP binding AT-rich DNA
464 and HP1/CDP-2 binding H3K9me3 for heterochromatin silencing (39, 40), the HCHC complex may be the
465 only heterochromatic-specific HDAC in Neurospora. This explains the large number of HCHC mutants, but
466 not other HDACs, recovered from a selection displaying compromised heterochromatin and reduced $5^{m}C$
467 (90). Our data also suggest that unknown HAT(s) specifically acetylate heterochromatic H4K16 – with this
468 enrichment only being observable with compromised HDAC activity, such as in a Δ*cdp-2* strain – given that
469 euchromatic acetylation is minimally decreased in this genetic background. An intriguing possibility is that
470 Neurospora modulates HCHC HDAC activity to increase heterochromatic acetylation to rapidly modulate
471 genome organization at certain developmental or cell cycle stages, including S phase in which a more open
472 chromosome conformation exists in fission yeast (91). Conversely, hypoacetylation of mitotic chromatin is
473 required for chromosome condensation and segregation to daughter cells, yet following cytokinesis,
474 chromatin is rapidly acetylated (63, 64), suggesting that dynamic histone acetylation during the cell cycle
475 could be necessary for proper genome organization. Hyperacetylated chromatin at distant genomic loci can
476 also cluster into a novel subcompartment to increase gene expression in BRD4-NUT expressing oncogenic
477 cells (68), in an analogous manner to the increased contacts occurring between hyperacetylated, yet distant
478 heterochromatic regions in HCHC mutants that we observe. Together, changes in acetylation patterns may
479 differentially organize eukaryotic genomes as a general phenomenon of more open and accessible chromatin.
480 We also observe changes in H3K9me3 deposition in heterochromatin, with ~20% of AT-rich regions in
481 a Δ*cdp-2* strain losing H3K9me3, with unchanged deposition on the remaining heterochromatic loci, while
482 H3K9me3 levels are modestly enhanced at most AT-rich regions in a Δ*chap* strain. These data again highlight
483 the unique phenotypes of HCHC members. Currently, it is unclear why some AT-rich regions lose H3K9me3

484 in a Δ*cdp-2* strain, but our preliminary analysis excludes AT-rich region size and extent of AT-richness. It
485 remains possible that the subnuclear positioning of a region, the reduced pairing between repeats in regions
486 (92), or DNA motifs in the transposon relicts of individual regions (93) impact H3K9me3 deposition upon
487 CDP-2 loss. In contrast, the gain of H3K9me3 in a Δ*chap* strain may result from increased levels or activity of
488 the DCDC, which may be a stopgap mechanism to promote AT-rich region compaction through additional
489 HP1 binding sites. Increases of DCDC protein levels are not unique, as the DCDC subunits DIM-7 and DIM-9
490 increase in a *dim-3* strain to possibly rescue reduced H3K9me3 levels (94). Our data suggest that WT
491 heterochromatic nucleosomes are not saturated with H3K9me3, given that greater levels of H3K9me3 are
492 possible in some mutant HCHC strains. Moreover, previous work has shown that H3K9me3 changes can
493 impact levels of H3K27me2/3 in facultative heterochromatin. In DCDC deficient strains, H3K27me2/3
494 relocates to AT-rich genomic loci (95, 96) suggesting deficient H3K9me3 in constitutive heterochromatin
495 results in novel facultative heterochromatin patterns. While ChIP qPCR showed no H3K27me2/3 change at
496 a few loci in HCHC deletion strains (95), examination of the global enrichment of H3K27me2/3 in HCHC
497 deficient backgrounds would be prudent, given the changes in H3K9me3 deposition reported here.

498 Changes in H3K9me3 are most apparent in a Δ*cdp-2*;Δ*dim-2* double mutant strain, which like the single
499 Δ*cdp-2* mutant, has H3K9me3 loss at ~20% of AT-rich regions, but the remaining heterochromatic regions
500 gain considerable H3K9me3 enrichment despite similar H4K16 hyperacetylation as a single Δ*cdp-2* mutant,
501 suggesting the loss of $5^{m}C$ signals for this H3K9me3 increase. Importantly, the genome organization of the
502 double mutant is disordered: the AT-rich (formerly heterochromatic) regions no longer segregate from
503 euchromatin despite greater H3K9me3 deposition (and presumably HP1 binding). These results may explain
504 the severe growth defect of the Δ*cdp-2*;Δ*dim-2* strain (40): the improper positioning of AT-rich regions into
505 the nucleus center may allow aberrant transcription, especially considering heterochromatic-euchromatic
506 contacts mediate proper gene expression in filamentous fungi (16, 97). Perhaps the increased H3K9me3
507 enrichment in the Δ*cdp-2*;Δ*dim-2* strain is a "last resort" by the fungus to repress AT-rich region transcription
508 in the center of the nucleus: increased H3K9me3 and HP1 compaction could minimize RNA Pol II recruitment
509 to this mislocalized chromatin. A crucial, unanswered question is: "how is H3K9me3 enrichment increased?"
510 We hypothesize that reduced AT-rich region compaction, observed in both Δ*chap* and Δ*cdp-2*;Δ*dim-2* strains,

511 signals for increased H3K9me3 deposition. Consistent with this hypothesis, nucleosomal disorder in
512 intergenic regions of the Neurospora genome causes subtle increases in H3K9me3 in *dim-1* strains (98), yet
513 additional work is needed to assess this possibility in HCHC mutants.

514 Importantly, our double mutant Hi-C results suggests that cytosine methylation may help to maintain
515 chromatin compartmentalization by facilitating the segregation of heterochromatin from euchromatin when
516 AT-rich regions are hyperacetylated. Specifically, only in strains devoid of both CDP-2 and DIM-2 are AT-rich
517 heterochromatic regions more apt to contact euchromatin. This change in genome organization is not seen
518 in a single Δ*cdp-2* mutant, where silent and active chromatin remain segregated despite increases in inter-
519 heterochromatic region contacts. We speculate that the additional methyl groups on AT-rich DNA in a Δ*cdp-*
520 *2* strain allow heterochromatic regions to remain associated with the nuclear periphery, either by active
521 recruitment by a methyl-DNA binding protein (99, 100) or passively by Liquid-Liquid Phase Separation
522 (101). It seems plausible that loss of chromatin compartmentalization can only occur when heterochromatin
523 is compromised and that $5^{m}C$ may safeguard genome organization and function by maintaining chromatin
524 compartmentalization. Future experiments should discern if $5^{m}C$ has a similar role for maintaining genome
525 topology in fungal pathogens or higher eukaryotes.

526

527 **Materials and Methods**

528 The strains used for all experiments, the abbreviated Hi-C and ChIP-seq protocols, and the bioinformatic
529 methods are found in the online Materials and Methods, provided in Supplementary File 1. *In situ* Hi-C was
530 performed as in (16), using the program hicExplorer (71) to process mapped reads for building the contact
531 matrices, which were used for all downstream analyses and image generation. ChIP-seq performed as in (32,
532 98), with minor modifications. The complete *in situ* Hi-C protocol is provided in Supplementary File 2, while
533 the ChIP-seq protocol is found in Supplementary File 3.

534

535 **Data availability**

536 All *Neurospora crassa* strains are available upon request. The *in situ* Hi-C and ChIP-seq high-throughput
537 sequencing data are available in the NCBI GEO superseries accession number GSE232935, which includes

538 the ChIP-seq data accession number GSE232933 and the Hi-C data accession number GSE232934.

539

540 **Acknowledgements**

541 The authors wish to thank UCCS Andrew Reckard, Sara Rodriguez, Yulia Shtanko, Victoria Toscano, and
542 Farh Kaddar (UCCS) for assistance with library generation, preliminary data analysis, or critical reading of
543 the manuscript, Doug Turnbull and Jeff Bishop (University of Oregon Genomics and Cell Characterization
544 Core Facility) for Illumina library sequencing service, and all Klocko lab members as well as UCCS
545 Department of Chemistry & Biochemistry colleagues for helpful comments and discussions. Funding was
546 provided by start-up funds from the UCCS College of Letters, Arts, and Sciences and an Academic Research
547 Enhancement Award (AREA) grant from the National Institutes of Health (1R15GM140396-01) to A.D.K.

548

549 **References**

550 1. T. Cremer, C. Cremer, Chromosome territories, nuclear architecture and gene regulation in mammalian
551 cells. *Nat Rev Genet* **2**, 292–301 (2001).

552 2. T. Misteli, Beyond the Sequence: Cellular Organization of Genome Function. *Cell* **128**, 787–800 (2007).

553 3. J. Dekker, Gene Regulation in the Third Dimension. *Science* **319**, 1793–1794 (2008).

554 4. T. Sexton, G. Cavalli, The Role of Chromosome Domains in Shaping the Functional Genome. *Cell* **160**, 1049–
555 1059 (2015).

556 5. B. Bonev, G. Cavalli, Organization and function of the 3D genome. *Nat Rev Genet* **17**, 661–678 (2016).

557 6. M. Falk, *et al.*, Heterochromatin drives compartmentalization of inverted and conventional nuclei. *Nature*
558 **570**, 395–399 (2019).

559 7. A. J. Shatkin, E. L. Tatum, Electron Microscopy of *Neurospora crassa* Mycelia. *J Biophys Biochem Cytol* **6**,
560 423–426 (1959).

561 8. A. Buchwalter, J. M. Kaneshiro, M. W. Hetzer, Coaching from the sidelines: the nuclear periphery in genome
562 regulation. *Nat Rev Genet* **20**, 39–50 (2019).

563 9. S. Schoenfelder, *et al.*, Preferential associations between co-regulated genes reveal a transcriptional
564 interactome in erythroid cells. *Nat Genet* **42**, 53–61 (2010).

565 10. E. E. M. Furlong, M. Levine, Developmental enhancers and chromosome topology. *Science* **361**, 1341–
566 1345 (2018).

567 11. P. A. Northcott, *et al.*, Enhancer hijacking activates GFI1 family oncogenes in medulloblastoma. *Nature*
568 **511**, 428–34 (2014).

569 12. W. A. Flavahan, *et al.*, Insulator dysfunction and oncogene activation in IDH mutant gliomas. *Nature* **529**,
570 110–114 (2016).

571 13. Z. Xu, *et al.*, Structural variants drive context-dependent oncogene activation in cancer. *Nature*, 1–9
572 (2022).

573 14. E. Lieberman-Aiden, *et al.*, Comprehensive Mapping of Long-Range Interactions Reveals Folding
574 Principles of the Human Genome. *Science* **326**, 289–293 (2009).

575 15. S. S. P. Rao, *et al.*, A 3D Map of the Human Genome at Kilobase Resolution Reveals Principles of Chromatin
576 Looping. *Cell* **159**, 1665–1680 (2014).

577 16. S. Rodriguez, *et al.*, The genome organization of *Neurospora crassa* at high resolution uncovers principles
578 of fungal chromosome topology. *G3 Genes Genomes Genetics* (2022)
579 https:/doi.org/10.1093/g3journal/jkac053.

580 17. K. Luger, A. W. Mäder, R. K. Richmond, D. F. Sargent, T. J. Richmond, Crystal structure of the nucleosome
581 core particle at 2.8 Å resolution. *Nature* **389**, 251–260 (1997).

582 18. E. I. Campos, D. Reinberg, Histones: Annotating Chromatin. *Annu Rev Genet* **43**, 559–599 (2009).

583 19. J. R. Dixon, *et al.*, Topological Domains in Mammalian Genomes Identified by Analysis of Chromatin
584 Interactions. *Nature* **485**, 376–380 (2012).

585 20. J. Dekker, E. Heard, Structural and functional diversity of Topologically Associating Domains. *Febs Lett*
586 **589**, 2877–2884 (2015).

587 21. A. S. Hansen, C. Cattoglio, X. Darzacq, R. Tjian, Recent evidence that TADs and chromatin loops are
588 dynamic structures. *Nucleus* **9**, 20–32 (2018).

589 22. M. Imakaev, *et al.*, Iterative correction of Hi-C data reveals hallmarks of chromosome organization. *Nat*
590 *Methods* **9**, 999–1003 (2012).

591 23. T. Cremer, M. Cremer, Chromosome territories. *Csh Perspect Biol* **2**, a003889 (2010).

592 24. C. Hoencamp, *et al.*, 3D genomics across the tree of life reveals condensin II as a determinant of
593 architecture type. *Science* **372**, 984–989 (2021).

594 25. M. R. Speicher, N. P. Carter, The new cytogenetics: blurring the boundaries with molecular biology. *Nat*
595 *Rev Genet* **6**, 782–792 (2005).

596 26. A. D. Klocko, *et al.*, Normal chromosome conformation depends on subtelomeric facultative
597 heterochromatin in *Neurospora crassa*. *Proc Natl Acad Sci* **113**, 15048–15053 (2016).

598 27. J. M. Galazka, *et al.*, Neurospora chromosomes are organized by blocks of importin alpha-dependent
599 heterochromatin that are largely independent of H3K9me3. *Genome Res* **26**, 1069–1080 (2016).

600 28. D. E. Torres, A. T. Reckard, A. D. Klocko, M. F. Seidl, Nuclear genome organization in fungi: From gene
601 folding to Rabl chromosomes. *Fems Microbiol Rev* (2023) https:/doi.org/10.1093/femsre/fuad021.

602 29. J. E. Galagan, *et al.*, The genome sequence of the filamentous fungus *Neurospora crassa*. *Nature* **422**, 859–
603 868 (2003).

604 30. Z. A. Lewis, *et al.*, Relics of repeat-induced point mutation direct heterochromatin formation in
605 *Neurospora crassa*. *Genome Res* **19**, 427–437 (2009).

606 31. M. R. Rountree, E. U. Selker, DNA methylation and the formation of heterochromatin in *Neurospora crassa*.
607 *Heredity* **105**, 38–44 (2010).

608 32. K. Jamieson, M. R. Rountree, Z. A. Lewis, J. E. Stajich, E. U. Selker, Regional control of histone H3 lysine 27
609 methylation in Neurospora. *Proc Natl Acad Sci* **110**, 6027–6032 (2013).

610 33. V. T. Bicocca, T. Ormsby, K. K. Adhvaryu, S. Honda, E. U. Selker, ASH1-catalyzed H3K36 methylation drives
611 gene repression and marks H3K27me2/3-competent chromatin. *Elife* **7**, e41497 (2018).

612 34. H. Tamaru, *et al.*, Trimethylated lysine 9 of histone H3 is a mark for DNA methylation in *Neurospora*
613 *crassa*. *Nat Genet* **34**, 75–79 (2003).

614 35. E. U. Selker, J. N. Stevens, DNA methylation at asymmetric sites is associated with numerous transition
615 mutations. *Proc Natl Acad Sci* **82**, 8114–8118 (1985).

616 36. E. T. Wiles, E. U. Selker, H3K27 methylation: a promiscuous repressive chromatin mark. *Curr Opin Genet*
617 *Dev* **43**, 31–37 (2017).

618 37. E. U. Selker, *et al.*, The methylated component of the *Neurospora crassa* genome. *Nature* **422**, 893–897
619 (2003).

620 38. Z. A. Lewis, *et al.*, DNA Methylation and Normal Chromosome Behavior in Neurospora Depend on Five
621 Components of a Histone Methyltransferase Complex, DCDC. *Plos Genet* **6**, e1001196 (2010).

622 39. S. Honda, *et al.*, Dual chromatin recognition by the histone deacetylase complex HCHC is required for
623 proper DNA methylation in *Neurospora crassa*. *Proc Natl Acad Sci* **113**, E6135–E6144 (2016).

624 40. S. Honda, *et al.*, Heterochromatin protein 1 forms distinct complexes to direct histone deacetylation and
625 DNA methylation. *Nat Struct Mol Biol* **19**, 471–477 (2012).

626 41. K. M. Smith, *et al.*, H2B- and H3-Specific Histone Deacetylases Are Required for DNA Methylation in
627 *Neurospora crassa*. *Genetics* **186**, 1207–1216 (2010).

628 42. H. Foss, C. Roberts, K. Claeys, E. Selker, Abnormal chromosome behavior in Neurospora mutants defective
629 in DNA methylation. *Science* **262**, 1737–1741 (1993).

630 43. T. Mizuguchi, *et al.*, Cohesin-dependent globules and heterochromatin shape 3D genome architecture in
631 S. pombe. *Nature* **516**, 432–435 (2014).

632 44. S. I. S. Grewal, S. Jia, Heterochromatin revisited. *Nat Rev Genetics* **8**, 35–46 (2007).

633 45. A. J. Courtney, A. R. Ferraro, A. D. Klocko, Z. A. Lewis, "Chromatin Structure and Function in *Neurospora*
634 *crassa*." in *The Mycota, A Comprehensive Treatise on Fungi as Experimental Systems, Third Edition for Basic*
635 *and Applied Research, Genetics and Biotechnology*, J. P. Benz, K. Schipper, Eds. (Springer Nature Switzerland
636 AG, 2020), pp. 3–24.

637 46. T. Jenuwein, C. D. Allis, Translating the Histone Code. *Science* **293**, 1074–1080 (2001).

638 47. F. Zenk, *et al.*, HP1 drives *de novo* 3D genome reorganization in early Drosophila embryos. *Nature* **593**,
639 289–293 (2021).

640 48. A. Eberharter, P. B. Becker, Histone acetylation: a switch between repressive and permissive chromatin.
641 *Embo Rep* **3**, 224–229 (2002).

642 49. Y.-J. C. Chen, E. Koutelou, S. Y. R. Dent, Now open: Evolving insights to the roles of lysine acetylation in
643 chromatin organization and function. *Mol Cell* **82**, 716–727 (2022).

644 50. D. M. Thurtle, J. Rine, The molecular topography of silenced chromatin in *Saccharomyces cerevisiae*. *Gene*
645 *Dev* **28**, 245–258 (2014).

646 51. B. J. E. Martin, *et al.*, Transcription shapes genome-wide histone acetylation patterns. *Nat Commun* **12**,
647 210 (2021).

648 52. J. N. McKnight, J. W. Boerma, L. L. Breeden, T. Tsukiyama, Global Promoter Targeting of a Conserved Lysine
649 Deacetylase for Transcriptional Shutoff during Quiescence Entry. *Mol Cell* **59**, 732–743 (2015).

650 53. A. R. Ferraro, *et al.*, Chromatin accessibility profiling in *Neurospora crassa* reveals molecular features
651 associated with accessible and inaccessible chromatin. *Bmc Genomics* **22**, 459 (2021).

652 54. T. Conrad, F. M. G. Cavalli, J. M. Vaquerizas, N. M. Luscombe, A. Akhtar, Drosophila Dosage Compensation
653 Involves Enhanced Pol II Recruitment to Male X-Linked Promoters. *Science* **337**, 742–746 (2012).

654 55. S. Fox, *et al.*, Hyperacetylated chromatin domains mark cell type-specific genes and suggest distinct
655 modes of enhancer function. *Nat Commun* **11**, 4544 (2020).

656 56. I. Dunham, *et al.*, An integrated encyclopedia of DNA elements in the human genome. *Nature* **489**, 57–74
657 (2012).

658 57. D. U. Gorkin, *et al.*, An atlas of dynamic chromatin landscapes in mouse fetal development. *Nature* **583**,
659 744–751 (2020).

660 58. E. Seto, M. Yoshida, Erasers of Histone Acetylation: The Histone Deacetylase Enzymes. *Csh Perspect Biol*
661 **6**, a018713 (2014).

662 59. A. J. Rubin, *et al.*, Lineage-specific dynamic and pre-established enhancer–promoter contacts cooperate
663 in terminal differentiation. *Nat Genet* **49**, 1522–1528 (2017).

664 60. R. Siersbæk, *et al.*, Dynamic Rewiring of Promoter-Anchored Chromatin Loops during Adipocyte
665 Differentiation. *Mol Cell* **66**, 420-435.e5 (2017).

666 61. M. W. G. Schneider, *et al.*, A mitotic chromatin phase transition prevents perforation by microtubules.
667 *Nature* **609**, 183–190 (2022).

668 62. A. Zhiteneva, *et al.*, Mitotic post-translational modifications of histones promote chromatin compaction
669 in vitro. *Open Biol* **7**, 170076 (2017).

670 63. B. J. Wilkins, *et al.*, A Cascade of Histone Modifications Induces Chromatin Condensation in Mitosis. *Science*
671 **343**, 77–80 (2014).

672 64. M. J. Kruhlak, *et al.*, Regulation of Global Acetylation in Mitosis through Loss of Histone Acetyltransferases
673 and Deacetylases from Chromatin*. *J Biol Chem* **276**, 38307–38319 (2001).

674 65. D. Cimini, M. Mattiuzzo, L. Torosantucci, F. Degrassi, Histone Hyperacetylation in Mitosis Prevents Sister
675 Chromatid Separation and Produces Chromosome Segregation Defects. *Mol Biol Cell* **14**, 3821–3833 (2003).

676 66. B. Pelham-Webb, *et al.*, H3K27ac bookmarking promotes rapid post-mitotic activation of the pluripotent
677 stem cell program without impacting 3D chromatin reorganization. *Mol Cell* **81**, 1732-1748.e8 (2021).

678 67. H. Kang, *et al.*, Dynamic regulation of histone modifications and long-range chromosomal interactions
679 during postmitotic transcriptional reactivation. *Gene Dev* **34**, 913–930 (2020).

680 68. C. D. Rosencrance, *et al.*, Chromatin Hyperacetylation Impacts Chromosome Folding by Forming a Nuclear
681 Subcompartment. *Mol Cell* **78**, 112-126.e12 (2020).

682 69. B. A. Gibson, *et al.*, Organization of Chromatin by Intrinsic and Regulated Phase Separation. *Cell* **179**, 470-
683 484.e21 (2019).

684 70. P. A. Knight, D. Ruiz, A fast algorithm for matrix balancing. *Ima J Numer Anal* **33**, 1029–1047 (2013).

685 71. F. Ramírez, *et al.*, High-resolution TADs reveal DNA sequences underlying genome organization in flies.
686 *Nat Commun* **9**, 189 (2018).

687 72. J. T. Robinson, *et al.*, Integrative genomics viewer. *Nat Biotechnol* **29**, 24–6 (2011).

688 73. N. Bonhoure, *et al.*, Quantifying ChIP-seq data: a spiking method providing an internal reference for
689 sample-to-sample normalization. *Genome Res* **24**, 1157–68 (2014).

690 74. B. Hu, *et al.*, Biological chromodynamics: a general method for measuring protein occupancy across the
691 genome by calibrating ChIP-seq. *Nucleic Acids Res* **43**, gkv670 (2015).

692 75. D. A. Orlando, *et al.*, Quantitative ChIP-Seq Normalization Reveals Global Modulation of the Epigenome.
693 *Cell Reports* **9**, 1163–1170 (2014).

694 76. D. Moazed, A. Kistler, A. Axelrod, J. Rine, A. D. Johnson, Silent information regulator protein complexes in
695 Saccharomyces cerevisiae: A SIR2/SIR4 complex and evidence for a regulatory domain in SIR4 that inhibits
696 its interaction with SIR3. *Proc Natl Acad Sci* **94**, 2186–2191 (1997).

697 77. S. Imai, C. M. Armstrong, M. Kaeberlein, L. Guarente, Transcriptional silencing and longevity protein Sir2
698 is an NAD-dependent histone deacetylase. *Nature* **403**, 795–800 (2000).

699 78. J. Wu, A. A. Carmen, R. Kobayashi, N. Suka, M. Grunstein, HDA2 and HDA3 are related proteins that interact
700 with and are essential for the activity of the yeast histone deacetylase HDA1. *Proc Natl Acad Sci* **98**, 4391–
701 4396 (2001).

702 79. S. E. Rundlett, *et al.*, HDA1 and RPD3 are members of distinct yeast histone deacetylase complexes that
703 regulate silencing and transcription. *Proc Natl Acad Sci* **93**, 14503–14508 (1996).

704 80. M. J. Carrozza, *et al.*, Histone H3 Methylation by Set2 Directs Deacetylation of Coding Regions by Rpd3S
705 to Suppress Spurious Intragenic Transcription. *Cell* **123**, 581–592 (2005).

706 81. Z. Guo, *et al.*, Structure of a SIN3–HDAC complex from budding yeast. *Nat Struct Mol Biol*, 1–8 (2023).

707 82. D. Kadosh, K. Struhl, Repression by Ume6 Involves Recruitment of a Complex Containing Sin3
708 Corepressor and Rpd3 Histone Deacetylase to Target Promoters. *Cell* **89**, 365–371 (1997).

709 83. T. Sugiyama, *et al.*, SHREC, an Effector Complex for Heterochromatic Transcriptional Silencing. *Cell* **128**,
710 491–504 (2007).

711 84. G. Job, *et al.*, SHREC Silences Heterochromatin via Distinct Remodeling and Deacetylation Modules. *Mol*
712 *Cell* **62**, 207–221 (2016).

713 85. T. Yamada, W. Fischle, T. Sugiyama, C. D. Allis, S. I. S. Grewal, The Nucleation and Maintenance of
714 Heterochromatin by a Histone Deacetylase in Fission Yeast. *Mol Cell* **20**, 173–185 (2005).

715 86. M. Freitag, P. C. Hickey, T. K. Khlafallah, N. D. Read, E. U. Selker, HP1 Is Essential for DNA Methylation in
716 Neurospora. *Mol Cell* **13**, 427–434 (2004).

717 87. S. A. Jacobs, S. Khorasanizadeh, Structure of HP1 Chromodomain Bound to a Lysine 9-Methylated Histone
718 H3 Tail. *Science* **295**, 2080–2083 (2002).

719 88. A. J. Bannister, T. Kouzarides, Regulation of chromatin by histone modifications. *Cell Res* **21**, 381–395
720 (2011).

721 89. T. Zhang, S. Cooper, N. Brockdorff, The interplay of histone modifications – writers that read. *Embo Rep*
722 **16**, 1467–1481 (2015).

723 90. A. D. Klocko, *et al.*, Selection and Characterization of Mutants Defective in DNA Methylation in *Neurospora*
724 *crassa*. *Genetics* **216**, genetics.303471.2020 (2020).

725 91. H. Tanizawa, K.-D. Kim, O. Iwasaki, K. Noma, Architectural alterations of the fission yeast genome during
726 the cell cycle. *Nat Struct Mol Biol* **24**, 965–976 (2017).

727 92. N. Rhoades, *et al.*, Recombination-independent recognition of DNA homology for meiotic silencing in
728 *Neurospora crassa*. *Proc Natl Acad Sci* **118**, e2108664118 (2021).

729 93. D. Nguyen, *et al.*, Transposon- and Genome Dynamics in the Fungal Genus Neurospora: Insights from
730 Nearly Gapless Genome Assemblies. *Fungal Genetics Reports* **66** (2022).

731 94. A. D. Klocko, *et al.*, Neurospora Importin α Is Required for Normal Heterochromatic Formation and DNA
732 Methylation. *Plos Genet* **11**, e1005083 (2015).

733 95. K. Jamieson, *et al.*, Loss of HP1 causes depletion of H3K27me3 from facultative heterochromatin and gain
734 of H3K27me2 at constitutive heterochromatin. *Genome Res* **26**, 97–107 (2016).

735 96. E. Y. Basenko, *et al.*, Genome-wide redistribution of H3K27me3 is linked to genotoxic stress and defective
736 growth. *Proc Natl Acad Sci* **112**, E6339–E6348 (2015).

737 97. H. M. Kramer, D. E. Cook, G. C. M. van den Berg, M. F. Seidl, B. P. H. J. Thomma, Three putative DNA
738 methyltransferases of *Verticillium dahliae* differentially contribute to DNA methylation that is dispensable
739 for growth, development and virulence. *Epigenet Chromatin* **14**, 21 (2021).

740 98. A. D. Klocko, *et al.*, Nucleosome Positioning by an Evolutionarily Conserved Chromatin Remodeler
741 Prevents Aberrant DNA Methylation in Neurospora. *Genetics* **211**, 563–578 (2019).

742 99. R. Meehan, J. D. Lewis, A. P. Bird, Characterization of MeCP2, a vertebrate DNA binding protein with
743 affinity for methylated DNA. *Nucleic Acids Res* **20**, 5085–5092 (1992).

744 100. E. U. Selker, *et al.*, Induction and maintenance of nonsymmetrical DNA methylation in Neurospora. *Proc*
745 *Natl Acad Sci* **99**, 16485–16490 (2002).

746 101. A. R. Strom, *et al.*, Phase separation drives heterochromatin domain formation. *Nature* **547**, 241–245
747 (2017).

748

749 **Figure Legends**

750 ***Figure 1.* Δcdp-2 *and* Δchap *strains change the genome organization of a single chromosome in***
751 **Neurospora crassa.** (A-B) Heatmap of contact probabilities of 20 kb bins across LG II of a (A) wild type (WT)
752 *Neurospora crassa* strain (16) or a (B) Δ*cdp-2* strain. Counts of raw reads of heterochromatin-specific *Mse*I
753 Hi-C are above the diagonal, while Knight Ruiz corrected (70, 71) read counts of euchromatin-specific *Dpn*II
754 Hi-C presented here and throughout this work (unless otherwise described). Bin numbers (vertical axis) and
755 genomic distance, in Megabases (Mb), (horizontal axis) are indicated. The scale bar shows the $\log_{10}$ number
756 of mapped reads per bin. Integrative Genomics Viewer (IGV) (72) image of WT CenH3 (red) and/or H3K9me3
757 (green) ChIP-seq tracks show the WT centromeres and heterochromatic regions, respectively; ChIP-seq
758 enrichment scales shown. Solid arrowheads in B. show increased inter-heterochromatic region contacts;
759 open arrowheads show decreased heterochromatic-euchromatic contacts. (C) The fold change in contact
760 strength ($\log_2$ scale) in a Δ*cdp-2* strain relative to a normalized WT strain of *Mse*I *in situ* Hi-C (above diagonal)
761 or *Dpn*II *in situ* Hi-C (below diagonal) datasets; purple line indicates the region in D. The open arrowhead
762 shows a heterochromatic region gaining internal contacts at the expense of euchromatic contacts. (D)
763 Heatmap of contact probability changes between distant heterochromatic regions and the centromere across
764 LG II in a Δ*cdp-2* strain relative to a WT strain at 10 kb resolution. WT H3K9me3 enrichment image below.

765 (E) Quantification of strongly increased, intra-chromosomal contacts in Δ*cdp-2* or Δ*chap* datasets, relative to
766 normalized WT strains, of bins enriched with the indicated histone PTMs; percentages indicate amount of all
767 bins enriched for the first histone PTM enriched with the second histone PTM. (F) Heatmap of contact
768 probabilities of Δ*chap* strain relative to a WT strain, as in A. (G) Heatmap of contact probability changes
769 between a Δ*chap* strain relative to a WT strain, as in C.
770
771 ***Figure 2.* Δcdp-2 *and* Δchap *strains alter the genome organization across the entire* Neurospora crassa**
772 ***genome.*** (A-B) The fold change in contact strength of 20 kb bins between LG II and LG III in (A) a Δ*cdp-2* or
773 (B) a Δ*chap* strain, relative to a WT strain of *Mse*I *in situ* Hi-C datasets. (C) Quantification of strongly
774 increased, inter-chromosomal contacts in Δ*cdp-2* or Δ*chap* datasets relative to a WT strain, as in Figure 1E.
775
776 ***Figure 3. Loss of CDP-2 alters the acetylation of H4K16, and causes some H3K9me3 loss, in constitutive***
777 ***heterochromatic regions across the* Neurospora crassa *genome.*** (A) IGV images of H3K9me3, H4K16ac,
778 and H3K9ac ChIP-seq enrichment tracks from WT and Δ*cdp-2* strains across LG II (top) and the LG II right
779 arm (bottom). SET-2 specific H3K27ac (assayed in a Δ*ash1*^{Y833F} strain (33)) shows euchromatin. Arrowheads
780 highlight heterochromatic regions gaining H4K16ac enrichment, while asterisks show AT-rich regions losing
781 H3K9me3, in Δ*cdp-2*. (B-C) Average enrichment profiles (top) and heatmaps (bottom) of the (B) H4K16ac or
782 (C) H3K9me3 enrichment in WT and Δ*cdp-2* strains over WT-defined H3K9me3-marked constitutive
783 heterochromatic regions (16). (D) Heatmaps showing the change in contact probability between Δ*cdp-2* and
784 WT *Mse*I datasets of a region on LG I in which several AT-rich loci lose H3K9me3 in a Δ*cdp-2* strain. H3K9me3
785 and/or H4K16ac ChIP-seq track images shown with each heatmap. Asterisks indicate regions losing
786 H3K9me3, pink arrowheads show the gain of H4K16ac in a Δ*cdp-2* strain, and black arrowheads highlight
787 gains in inter-heterochromatic region contacts in a Δ*cdp-2* strain.
788
789 ***Figure 4. Constitutive heterochromatic regions have increased H4K16ac and H3K9me3 enrichment***
790 ***with CDP-2 and DIM-2 loss.*** (A) Images of H3K9me3 and H4K16ac ChIP-seq enrichment tracks of WT, Δ*cdp-*
791 *2*, and Δ*cdp-2;*Δ*dim-2* strains, displayed on IGV, as in Figure 3A. Asterisks indicate AT-rich regions losing

792 H3K9me3 enrichment in both Δ*cdp-2* and Δ*cdp-2;*Δ*dim-2* strains. (B-C) Average enrichment profiles (top)
793 and heatmaps (bottom) of (B) H4K16ac or (C) H3K9me3 enrichment in WT, Δ*cdp-2*, and Δ*cdp-2;*Δ*dim-2*
794 strains over the H3K9me3-marked constitutive heterochromatic regions defined in a WT strain.
795
796 ***Figure 5. The genome organization of a* Δcdp-2;Δdim-2 *strain gains heterochromatic-euchromatic***
797 ***contacts.*** (A,C) The fold change in contact strength of LG II in a Δ*cdp-2*;Δ*dim-2* strain relative to a (A) WT
798 strain or (C) Δ*cdp-2* strain of *Dpn*II *in situ* Hi-C, as in Figure 1C. Arrowheads indicate the heterochromatic
799 regions highlighted in Figure 5D. (B) Quantification of strongly changed intra-chromosomal (top) or inter-
800 chromosomal (bottom) contacts in Δ*cdp-2* or Δ*cdp-2*;Δ*dim-2* strains relative to a WT strain, as in Figure 1E.
801 (D) The fold change in raw contact strength of two heterochromatic regions in a Δ*cdp-2*;Δ*dim-2* strain relative
802 to a (top) WT or (bottom) Δ*cdp-2* strain. IGV image of H3K9me3 enrichment of Δ*cdp-2* or Δ*cdp-2*;Δ*dim-2*
803 strains, as well as genes, are shown in the middle.
804
805 ***Figure 6. The models of how HCHC loss impacts heterochromatin formation and genome organization***
806 ***in* Neurospora crassa*.*** (A-D) In WT or HCHC mutant strains, heterochromatin formation at the level of
807 nucleosomes (left) and organization of two example chromosomes (right) are displayed. (A) In a WT strain,
808 the HCHC (HDA-1, CDP-2, HP1, CHAP) complex removes the acetylation marks (green triangles) from histone
809 tails; CDP-2 can bind H3K9me3 (red hexagons) and recruits HDA-1 to AT-rich DNA (orange lines), while
810 CHAP interacts with distant nucleosomes in AT-rich regions. On deacetylated histone tails, the DCDC (DIM-
811 5/7/9, CUL4, DDB1^{dim-8}, Complex) deposits H3K9me3, which is bound by HP1 to directly recruit the DNA
812 methyltransferase DIM-2 for 5^{m}C (orange hexagons). The action of both complexes establishes a Rabl
813 chromosome conformation characterized by a centromere (red circles) cluster on the nuclear periphery that
814 is distinct from (sub)telomeres bundles (green circles). Interspersed heterochromatic regions (black circles)
815 also associate at the nuclear periphery. (B) CDP-2 loss causes altered (here, gains) in 5^{m}C and histone
816 acetylation while maintaining H3K9me3 at most heterochromatic regions, all of which increases intra-
817 heterochromatic region contacts while decreasing inter-chromosomal centromeric contacts. (C) Loss of
818 CHAP relaxes heterochromatic region compaction and reduces some heterochromatic region interactions,

819 despite increases in $5^{m}C$ and H3K9me3. (D) Loss of both CDP-2 and DIM-2 causes gains in histone acetylation

820 and H3K9me3, but the genome gains disorder as heterochromatic regions interact more with euchromatin.

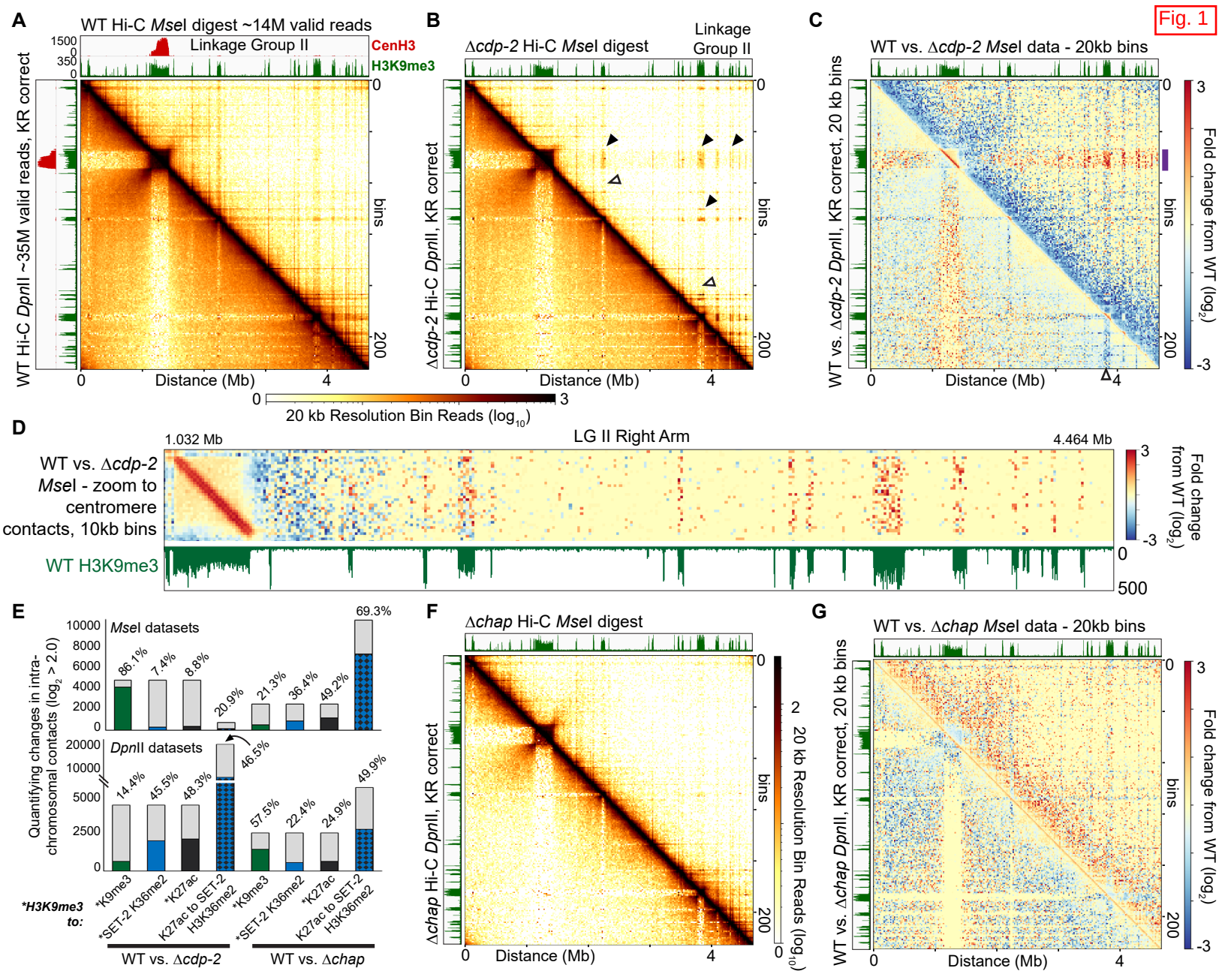
Fig. 1
A
WT Hi-C MseI digest ~14M valid reads
Linkage Group II
CenH3
H3K9me3
WT Hi-C DpnII ~35M valid reads, KR correct
bins
Distance (Mb)
B
Δcdp-2 Hi-C MseI digest
Linkage Group II
Δcdp-2 Hi-C DpnII, KR correct
C
WT vs. Δcdp-2 MseI data - 20kb bins
WT vs. Δcdp-2 DpnII, KR correct, 20 kb bins
Fold change from WT (log2)
20 kb Resolution Bin Reads (log10)
D
LG II Right Arm
1.032 Mb
4.464 Mb
WT vs. Δcdp-2 MseI - zoom to centromere contacts, 10kb bins
WT H3K9me3
Fold change from WT (log2)
E
MseI datasets
DpnII datasets
Quantifying changes in intra-chromosomal contacts (log2 > 2.0)
86.1%
7.4%
8.8%
20.9%
21.3%
36.4%
49.2%
69.3%
14.4%
45.5%
48.3%
46.5%
57.5%
22.4%
24.9%
49.9%
*H3K9me3 to:
*K9me3
*SET-2 K36me2
*K27ac
K27ac to SET-2 H3K36me2
WT vs. Δcdp-2
WT vs. Δchap
F
Δchap Hi-C MseI digest
Δchap Hi-C DpnII, KR correct
20 kb Resolution Bin Reads (log10)
G
WT vs. Δchap MseI data - 20kb bins
WT vs. Δchap DpnII, KR correct, 20 kb bins
Fold change from WT (log2)

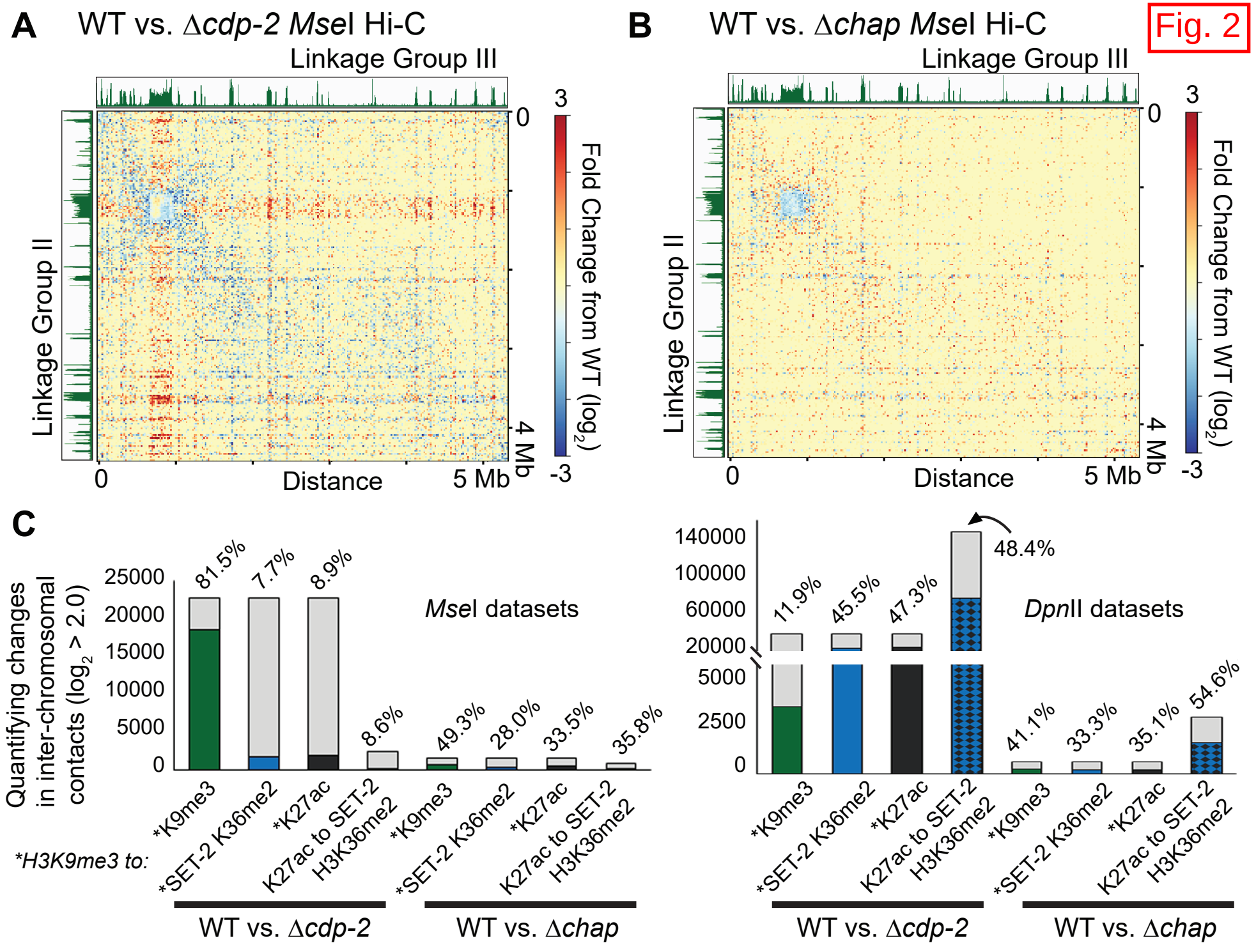
Fig. 2
A
WT vs. Δcdp-2 MseI Hi-C
Linkage Group III
Linkage Group II
Distance
0
5 Mb
4 Mb
3
-3
Fold Change from WT (log2)
B
WT vs. Δchap MseI Hi-C
Linkage Group III
Linkage Group II
Distance
0
5 Mb
4 Mb
3
-3
Fold Change from WT (log2)
C
Quantifying changes in inter-chromosomal contacts (log2 > 2.0)
MseI datasets
81.5%
7.7%
8.9%
8.6%
49.3%
28.0%
33.5%
35.8%
*K9me3
*SET-2 K36me2
*K27ac
K27ac to SET-2 H3K36me2
*H3K9me3 to:
WT vs. Δcdp-2
WT vs. Δchap
DpnII datasets
11.9%
45.5%
47.3%
48.4%
41.1%
33.3%
35.1%
54.6%

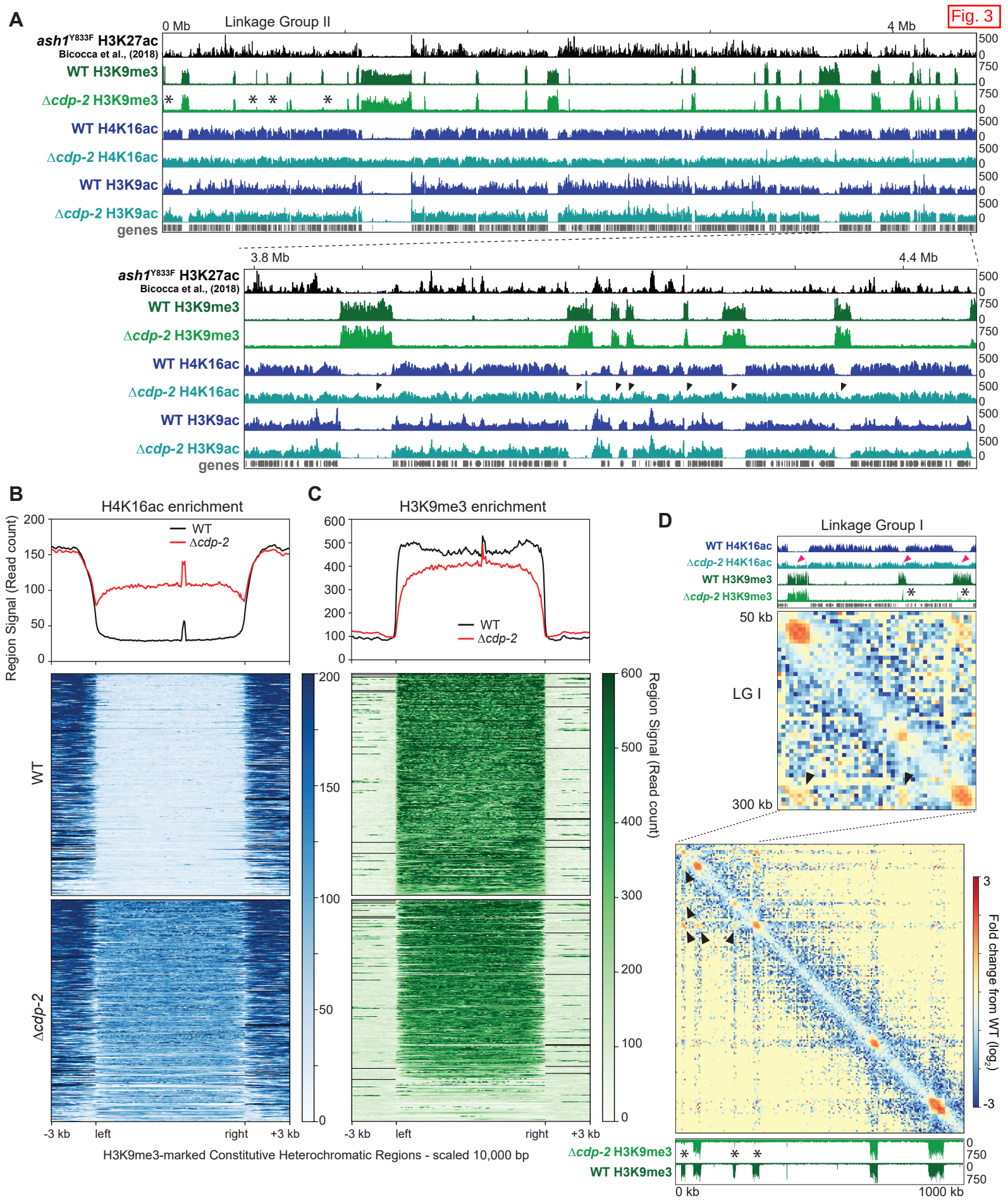
Fig. 3
A
Linkage Group II
0 Mb
4 Mb
ash1Y833F H3K27ac
Bicocca et al., (2018)
WT H3K9me3
Δcdp-2 H3K9me3
WT H4K16ac
Δcdp-2 H4K16ac
WT H3K9ac
Δcdp-2 H3K9ac
genes
3.8 Mb
4.4 Mb
B
H4K16ac enrichment
Region Signal (Read count)
WT
Δcdp-2
C
H3K9me3 enrichment
Region Signal (Read count)
-3 kb
left
right
+3 kb
H3K9me3-marked Constitutive Heterochromatic Regions - scaled 10,000 bp
D
Linkage Group I
50 kb
LG I
300 kb
Fold change from WT (log2)
0 kb
1000 kb

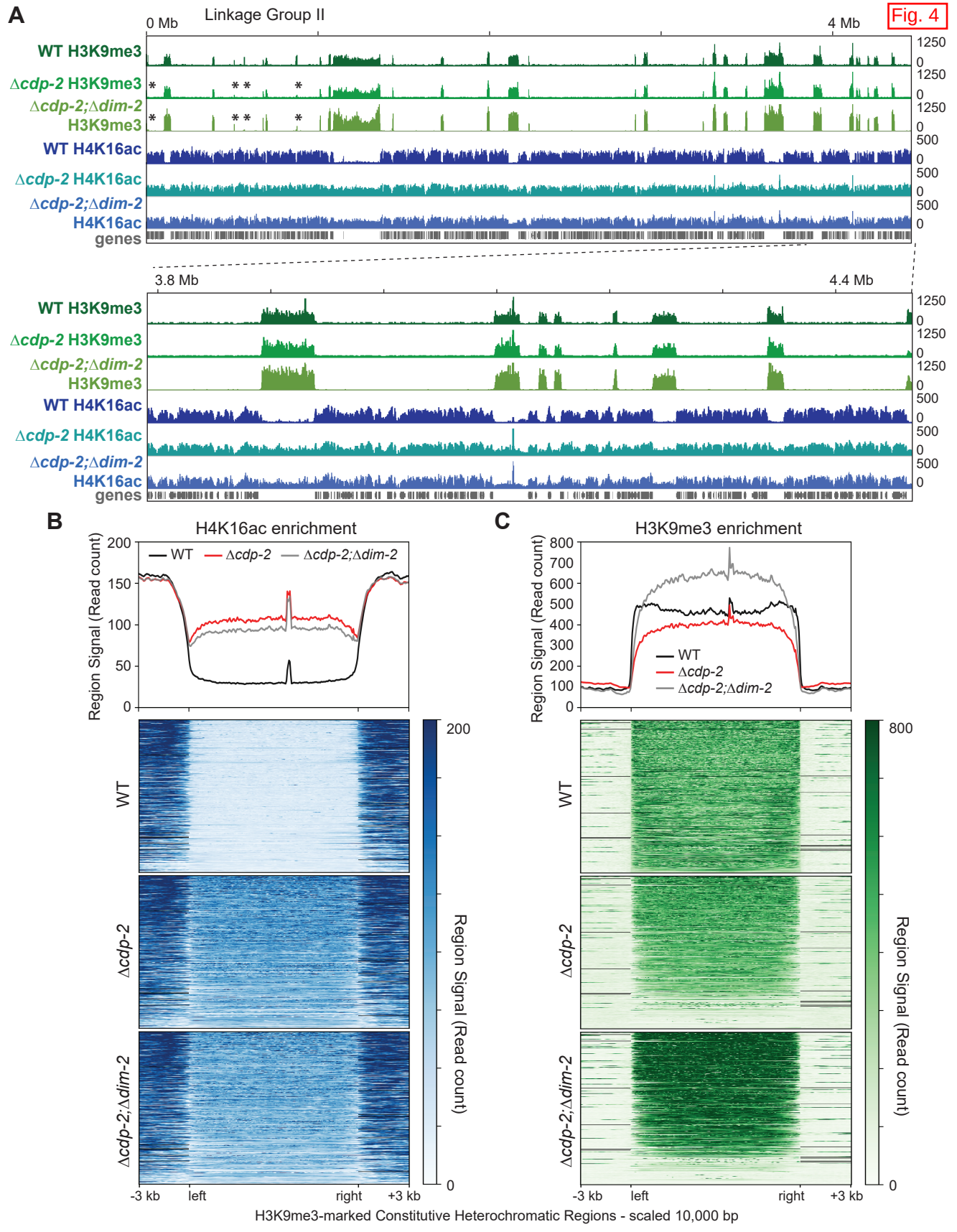
Fig. 4
A
Linkage Group II
0 Mb
4 Mb
WT H3K9me3
Δcdp-2 H3K9me3
Δcdp-2;Δdim-2 H3K9me3
WT H4K16ac
Δcdp-2 H4K16ac
Δcdp-2;Δdim-2 H4K16ac
genes
1250
500
0
3.8 Mb
4.4 Mb
B
H4K16ac enrichment
Region Signal (Read count)
WT
Δcdp-2
Δcdp-2;Δdim-2
200
150
100
50
0
-3 kb
left
right
+3 kb
C
H3K9me3 enrichment
800
700
600
500
400
300
200
100
H3K9me3-marked Constitutive Heterochromatic Regions - scaled 10,000 bp

Fig. 5

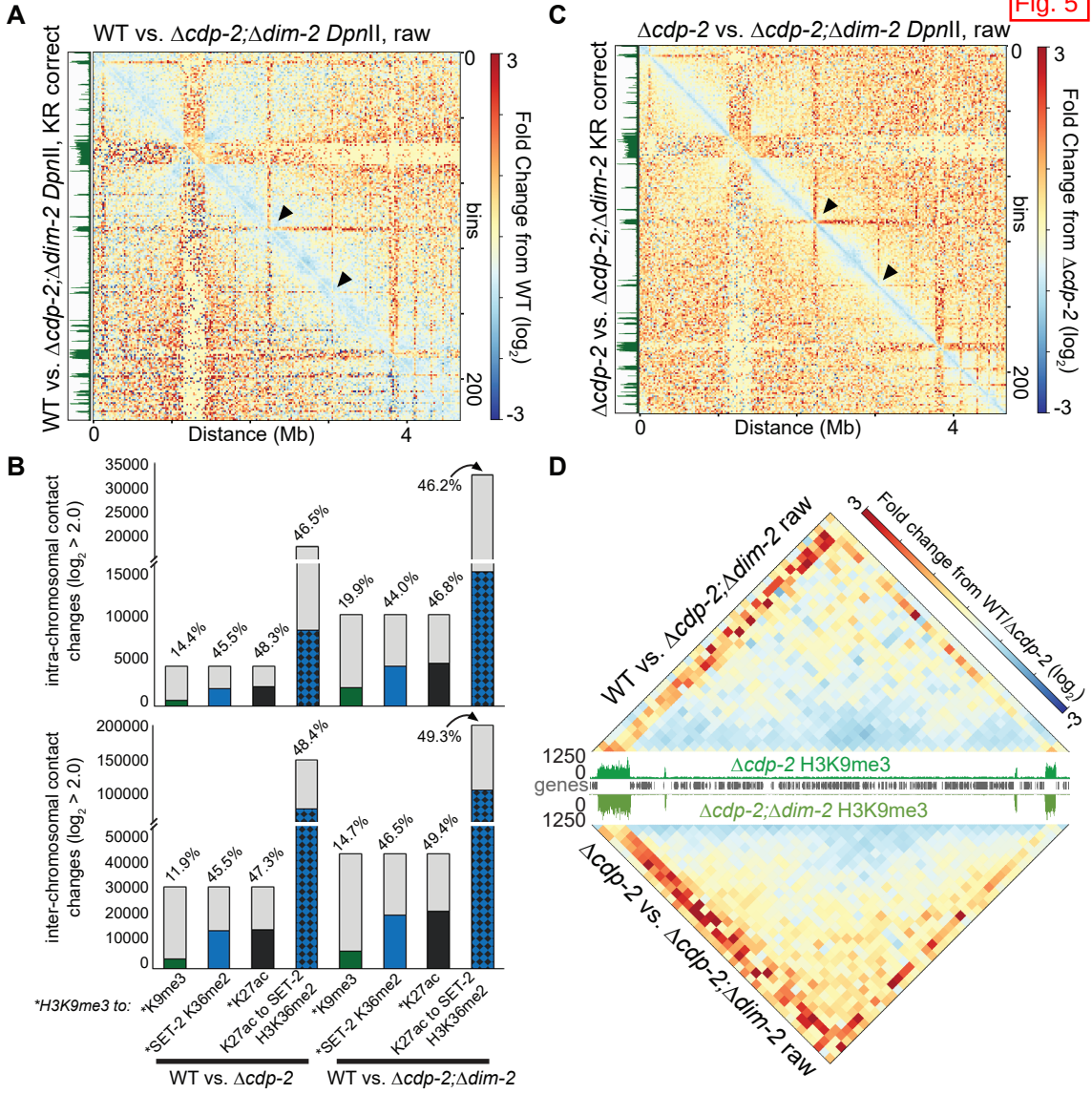
A
WT vs. Δcdp-2;Δdim-2 DpnII, raw
WT vs. Δcdp-2;Δdim-2 DpnII, KR correct
bins
Distance (Mb)
Fold Change from WT (log2)
C
Δcdp-2 vs. Δcdp-2;Δdim-2 DpnII, raw
Δcdp-2 vs. Δcdp-2;Δdim-2 KR correct
Fold Change from Δcdp-2 (log2)
B
intra-chromosomal contact changes (log2 > 2.0)
inter-chromosomal contact changes (log2 > 2.0)
14.4%
45.5%
48.3%
46.5%
19.9%
44.0%
46.8%
46.2%
11.9%
45.5%
47.3%
48.4%
14.7%
46.5%
49.4%
49.3%
*H3K9me3 to:
*K9me3
*SET-2 K36me2
*K27ac
K27ac to SET-2 H3K36me2
WT vs. Δcdp-2
WT vs. Δcdp-2;Δdim-2
D
WT vs. Δcdp-2;Δdim-2 raw
Fold change from WT/Δcdp-2 (log2)
Δcdp-2 H3K9me3
genes
Δcdp-2;Δdim-2 H3K9me3
Δcdp-2 vs. Δcdp-2;Δdim-2 raw

Fig. 6

A

Wildtype heterochromatin and genome organization

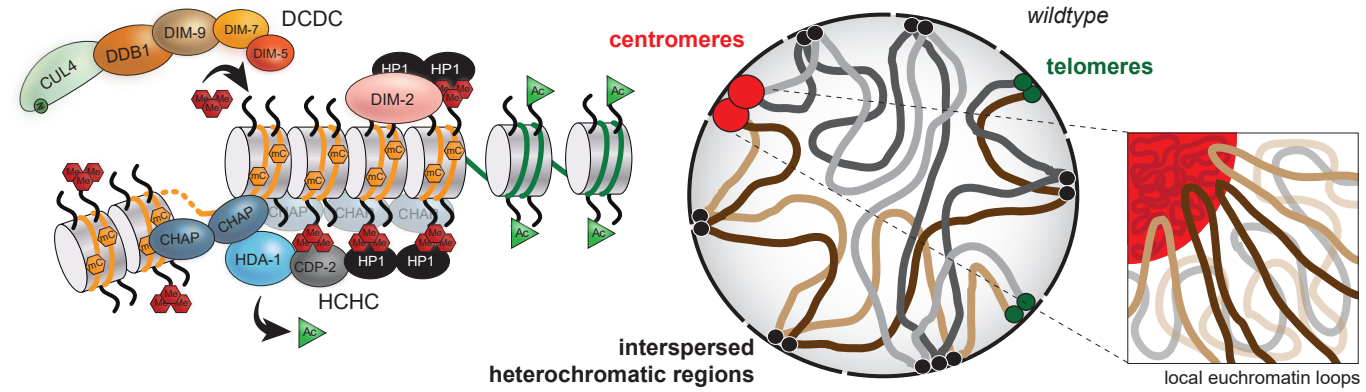

B

HCHC-deficient (Δ*cdp-2*) heterochromatin and genome organization

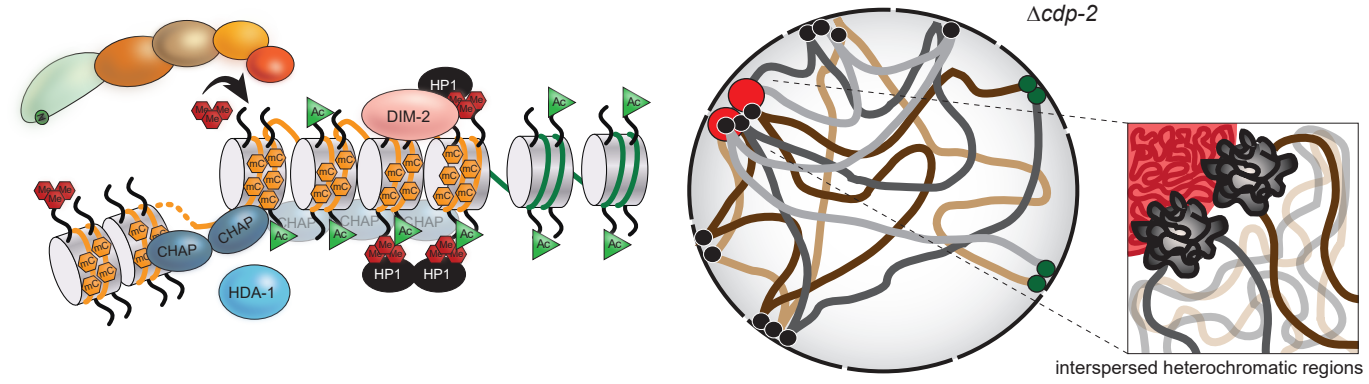

C

HCHC-deficient (Δ*chap*) heterochromatin and genome organization

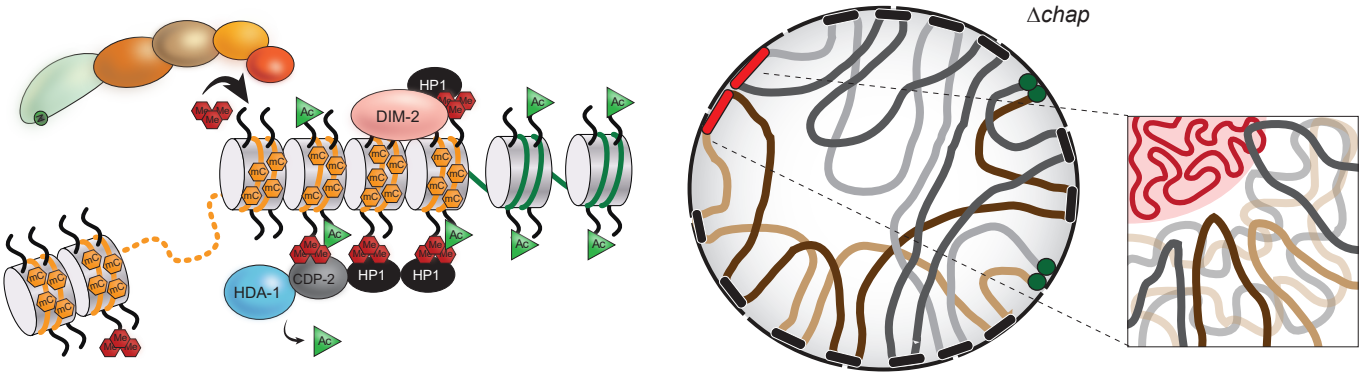

D
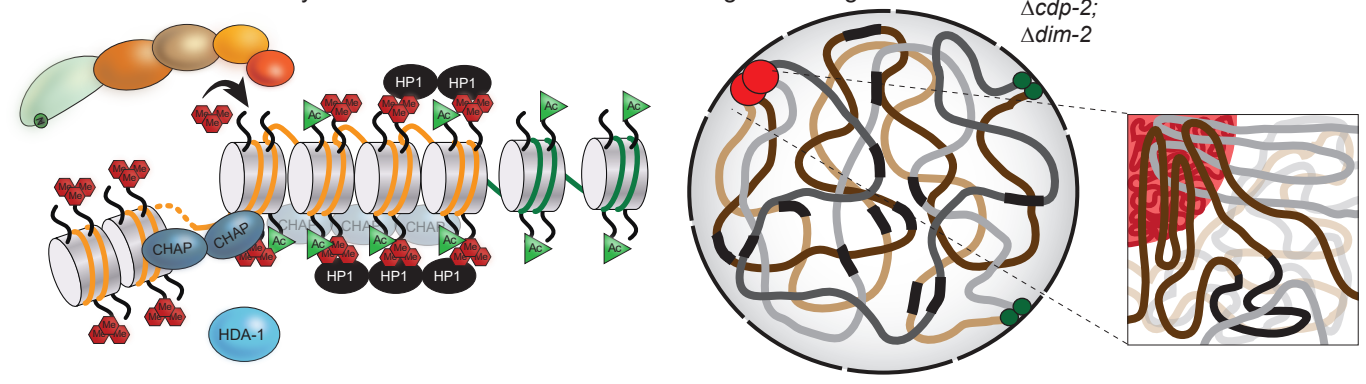
HCHC and DNA methylation-deficient heterochromatin and genome organization